Chemical Models of Atmospheric Chemistry on Hot Rocky Exoplanets

2nd EPSCOR Collaboration Meeting

4 – 6 August 2014

NASA Ames Research Center

Professor Bruce Fegley, Jr.

Planetary Chemistry Laboratory, Department of Earth & Planetary Sciences and

McDonnell Center for Space Sciences,

Washington University, St Louis, MO 63130 USA

Outline

Progress since last meeting

Some new directions

Summary of progess since last group meeting in August 2013
Professor Bruce Fegley, Jr., Washington University in St Louis

Refereed papers

Moynier, F. and **Fegley, B. Jr.** (2014) The Earth's Building Blocks, invited chapter submitted to AGU.

Lupu, R. E., Zahnle, K., Marley, M. S., Schaefer, L., **Fegley, B**., Morley, C., Cahoy, K., Freedman, R., & Fortney, J. J. (2014) The atmospheres of Earth –like planets after giant impact events. *ApJ*, 784:27 (19 pages) doi:10.1088/0004-637X/784/1/27

Fegley, B., Jr. and Schaefer, L. (2014) Chemistry of the Earth's Earliest Atmosphere, chapter 6.3 In *The Atmosphere – History* (ed., J. Farquhar), *Treatise on Geochemistry*, (eds. H. D. Holland and K. K. Turekian), Elsevier Science, 2nd ed http://dx.doi.org/10.1016/B978-0-08-095975-7.01303-6

Presentations

Schaefer, L. and **Fegley, B., Jr**. (2014) Chemical equilibrium models of the redox state of Earth's earliest atmosphere. Invited talk, session 03c: Climate and atmospheric evolution during the Hadean and Archean and comparison to other planets, June 2014 Goldschmidt meeting, Sacramento, CA

Ongoing work

Fractional vaporization of Na and K from anhydrous magmas

Solubility of lava planets in steam atmospheres

Olivine vaporization
– provide samples and advice to Nate Jacobson and Gustavo Costa

The Astrophysical Journal, 784:27 (19pp), 2014 March 20 doi:10.1088/0004-637X/784/1/27

THE ATMOSPHERES OF EARTHLIKE PLANETS AFTER GIANT IMPACT EVENTS

R. E. Lupu[1], Kevin Zahnle[2], Mark S. Marley[2], Laura Schaefer[3], Bruce Fegley[4], Caroline Morley[5], Kerri Cahoy[6], Richard Freedman[1], and Jonathan J. Fortney[5]
[1] SETI Institute/NASA Ames Research Center, Moffet Field, CA 94035, USA; Roxana.E.Lupu@nasa.gov
[2] NASA Ames Research Center, Moffet Field, CA 94035, USA
[3] Harvard/Smithsonian Center for Astrophysics, Cambridge, MA 02138, USA
[4] Planetary Chemistry Laboratory, Department of Earth & Planetary Sciences and McDonnell Center for the Space Sciences, Washington University, St. Louis, MO 63130, USA
[5] Department of Astronomy and Astrophysics, University of California, Santa Cruz, CA 95064, USA
[6] Massachusetts Institute of Technology, Cambridge, MA 02139, USA
Received 2013 August 2; accepted 2014 January 14; published 2014 February 28

ABSTRACT

It is now understood that the accretion of terrestrial planets naturally involves giant collisions, the moon-forming impact being a well-known example. In the aftermath of such collisions, the surface of the surviving planet is very hot and potentially detectable. Here we explore the atmospheric chemistry, photochemistry, and spectral signatures of post-giant-impact terrestrial planets enveloped by thick atmospheres consisting predominantly of CO_2 and H_2O. The atmospheric chemistry and structure are computed self-consistently for atmospheres in equilibrium with hot surfaces with composition reflecting either the bulk silicate Earth (which includes the crust, mantle, atmosphere, and oceans) or Earth's continental crust. We account for all major molecular and atomic opacity sources including collision-induced absorption. We find that these atmospheres are dominated by H_2O and CO_2, while the formation of CH_4 and NH_3 is quenched because of short dynamical timescales. Other important constituents are HF, HCl, NaCl, and SO_2. These are apparent in the emerging spectra and can be indicative that an impact has occurred. The use of comprehensive opacities results in spectra that are a factor of two lower brightness temperature in the spectral windows than predicted by previous models. The estimated luminosities show that the hottest post-giant-impact planets will be detectable with near-infrared coronagraphs on the planned 30 m class telescopes. The 1–4 μm will be most favorable for such detections, offering bright features and better contrast between the planet and a potential debris disk. We derive cooling timescales on the order of 10^{5-6} yr on the basis of the modeled effective temperatures. This leads to the possibility of discovering tens of such planets in future surveys.

Key words: brown dwarfs – planetary systems – planets and satellites: general – radiative transfer – stars: low-mass

Online-only material: color figures

1. INTRODUCTION

The final assembly of terrestrial planets is now universally thought to have occurred through a series of giant impacts—essentially collisions between planets—spread out over some 100 million years (Cameron & Ward 1976; Wetherill 1985; Lissauer 1993; Chambers 2004; Raymond et al. 2004). The most famous of these is Earth's own moon-forming impact (Hartmann et al. 1986; Benz et al. 1986; Canup & Righter 2000; Canup & Asphaug 2001; Agnor & Asphaug 2004; Canup 2004). It takes at least 10 collisions between planets to make a Venus and an Earth, as not every collision results in a merger. In the aftermath of one of these collisions, the surviving planet is hot and can remain hot for millions of years (Zahnle 2006; Zahnle et al. 2007). During this phase of accretion, a prototerrestrial planet may have a dense steam atmosphere (e.g., Abe & Matsui 1988; Matsui & Abe 1986; Zahnle et al. 1988; Hashimoto et al. 2007; Schaefer & Fegley 2010). Eventually, the atmosphere cools and water vapor condenses into clouds. How long the stricken planet remains hot depends on the size of the collision and the nature of the planet's atmosphere. While hot, the planet will be bright, especially in the near-IR, where spectral windows reveal hotter atmospheric depths.

Such young, post-giant-impact terrestrial planets will be far brighter and easier to detect around nearby young stars than old, cold terrestrial planets (Stern 1994; Miller-Ricci et al. 2009). Furthermore, the time period after the last giant impact sets the boundary condition for the subsequent thermal evolution of Earth. Whether a terrestrial planet retains water or enters into a runaway greenhouse ultimately depends upon the conditions after the last giant impact (Hamano et al. 2013). The classic early studies of runaway greenhouse atmospheres (e.g., Ingersoll 1969) used a gray approximation for water opacity and neglected other opacity sources. Second-generation models that greatly improved on the radiative transfer in runaway and near-runaway greenhouse atmospheres were developed independently by Kasting (1988) and Abe & Matsui (1988). These models, state-of-the-art in their day, used multiple bands of H_2O and CO_2, but the description of hot bands was necessarily crude given what was known at the time. Furthermore, these models completely neglected other opacity sources, some of which (e.g., the alkali metals) are now known (thanks to brown dwarf science, e.g., Burrows et al. 2000) to be of first-order importance.

The composition of a postimpact atmosphere is unlikely to be a pure mixture of H_2O and CO_2. At a minimum, volatile species will evaporate and the atmosphere will equilibrate with the surface. Thus, the atmospheric composition depends upon the surface composition. Whether or not the surface is oxidized (Fe^{3+} minerals) versus reduced (Fe^{2+} minerals), for example, will control the oxidation state of carbon compounds in the atmosphere. Thus, any model of the atmospheric structure of a postimpact world must consider a range of surface compositions.

Radiometric dating shows that the Earth's continental crust (CC) formed very early in the history of the Earth. As noted by Fegley & Schaefer (2012), coupled modeling of the short-lived ^{182}Hf–^{182}W and ^{146}Sm–^{142}Nd systems by Moynier et al. (2010) shows Earth's crust formed 38–75 million years after the formation of the solar system. The oldest dated crustal samples are detrital zircons from Jack Hills, Australia, which are up to 4404 million years old (Wilde et al. 2001; Harrison et al. 2005). These zircons show that CC existed 164 million years after formation of the solar system. Thus, it is likely that earthlike rocky exoplanets also formed felsic crusts very early in their evolution. However, the alternative case that the surface of a postimpact world does not yet reflect the formation of continents and is composed mostly of mafic silicates, like the bulk silicate Earth (BSE), should also be considered.

In this paper we report on our calculation of the atmospheric thermal structure, equilibrium and disequilibrium chemistry, emergent spectra, and thermal evolution of post-giant-impact terrestrial planets. On the basis of these results, we also discuss the detectability of such worlds and the spectral markers that can discriminate between different surface chemistries. The framework we present is relevant to a variety of problems, including the runaway greenhouse and the early evolution of the Earth–Moon system. We necessarily neglect some processes that might be important, such as cloud formation and a self-consistent photochemical model, which are deferred to a future paper.

2. MODELING

To model the atmospheric thermal structure of postimpact worlds, we construct a suite of radiative–convective equilibrium models that are consistent with a specified range of surface temperatures. For each model, we specify the incident flux, surface gravity and pressure, and surface chemical composition. We note that the impacted planet cools over a timescale of 10^5–10^6 yr (Zahnle et al. 2007), while the timescale for atmospheric adjustment to radiative and convective equilibrium is far shorter, in the range of a day or so. Thus, even though the atmosphere will cool through time, the thermal structure for a given surface temperature is well defined. This is the same procedure that is commonly used for evolution calculations for gas giants where a single atmospheric boundary is associated with a cooling planet or brown dwarf.

For a specified surface temperature, we solve for the radiative–convective $T-p$ profile by taking into account the heating from the surface and the incoming solar radiation, ensuring energy balance throughout the atmosphere. The atmosphere code we employ iteratively solves for radiative–convective equilibrium by adjusting the size of the convection zone until the lapse rate everywhere in the convective region is sub-adiabatic. This code was originally developed for modeling Titan's atmosphere (McKay et al. 1989) and has been extensively modified and applied to the study of brown dwarfs (e.g., Marley et al. 1996; Cushing et al. 2008; Saumon & Marley 2008) and solar and extrasolar giant planets (Marley et al. 1999; Marley & McKay 1999; Fortney et al. 2008a, 2008b). When fully converged, the radiative layers are typically in full radiative energy balance to about 1 part in 10^5. Our solution achieves this energy balance by using a matrix method that progressively adjusts an initial guess at the $T-p$ profile (Pollack & Ohring 1973; McKay et al. 1989) rather than by time stepping (e.g., Gierasch & Goody 1968; Pavlov et al. 2000). Both approaches are intrinsically quasi-static, with the matrix method being more efficient (e.g., Ramanathan & Coakley 1978).

Table 1
Composition of Vaporized Material

Compound	Continental Crust[a,b] wt. (%)	Bulk Silicate Earth[b,c] wt. (%)
SiO_2	64.0	45.9
MgO	2.4	37.1
Al_2O_3	14.7	4.6
TiO_2	0.59	0.22
FeO	...	8.2
Fe_2O_3	4.9	...
CaO	4.1	3.7
Na_2O	2.9	0.35
K_2O	3.1	0.03
P_2O_5	0.17	...
MnO	0.08	...
Elemental breakdown		
H	0.045	0.006
C	0.199	0.006
N	0.006	0.88e-4
O	47.20	44.42
S	0.070	0.027
F	0.053	0.002
Cl	0.047	0.004
Si	28.80	21.61
Al	7.96	2.12
Fe	4.32	6.27
Ca	3.85	2.46
Na	2.36	0.29
Mg	2.20	22.01
K	2.14	0.02
Ti	0.401	0.12
P	0.076	0.008
Cr	0.013	0.29
Mn	0.072	0.11

Notes.
[a] Wedepohl (1995).
[b] Schaefer et al. (2012).
[c] Fegley & Schaefer (2012).

To derive the atmospheric composition, we rely on thermochemical equilibrium calculations for "earthlike" rocky planets that are heated to high temperatures (Schaefer et al. 2012). The chemistry calculations are done for a grid with temperatures from 300 to 4000 K and one microbar to 300 bar pressures by using a Gibbs energy minimization code (see van Zeggeren & Storey 1970). Approximately ~800 compounds (solid, liquid, gas) of the elements are included in the calculations. We use two reasonable representative compositions of the silicate portion of rocky planets: (1) the Earth's CC (Wedepohl 1995) and (2) the BSE (Kargel & Lewis 1993). These two compositions allow us to examine differences in atmospheres formed by outgassing of silica-rich (felsic) rocks—like the Earth's continental crust—and MgO- and FeO-rich (mafic) rocks—like the BSE. These compositions describe the class of rocky planets around stars of solar metallicity, with a differentiated Fe metal and FeS core. For reference, the BSE is the composition of the silicate portion of the Earth that evolved into the present-day mantle, crust, oceans, and atmosphere. The mantle makes up 99.4% by mass of the BSE; thus, the BSE composition is similar to that of Earth's mantle (Schaefer et al. 2012). The most important compounds considered in the calculations of CC and BSE compositions are listed in Table 1. The breakdown in terms

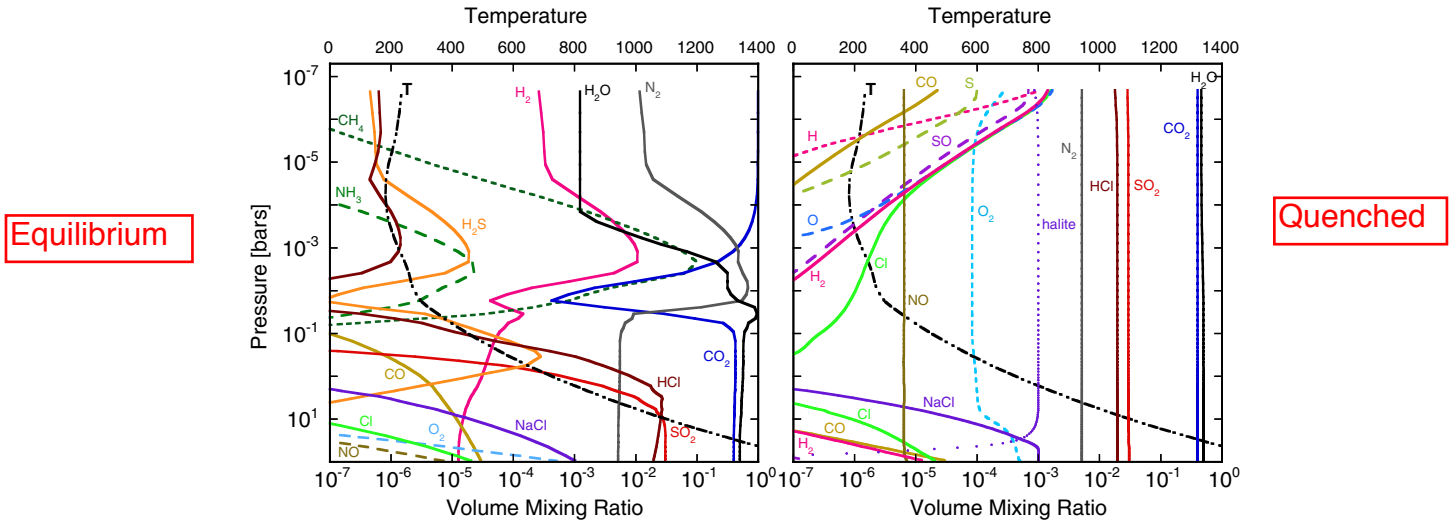

Figure 4. Chemical compositions of 100 bar atmospheres over a 1600 K surface in chemical equilibrium with the continental crust composition. The pressure–temperature profile for this model is shown with a dash-dotted black line, with the corresponding temperature axis at the top. Left: each level of the atmosphere equilibrates with the surface. Composition is sensitive to temperature. Geochemical volatiles Na, Cl, and S enter minerals. The profiles for CH_4 and NH_3 are shown with dashed lines, since their abundances become quenched at temperatures between 900 and 1000 K (see Section 4.1). Right: results from the photochemical kinetics model using K_{zz} computed from the convective heat flux. Composition is dominated by mixing at middle altitudes and photolysis at high altitudes. Hydrochloric acid, salt (halite), and various sulfur species are mixed through the atmosphere.

(A color version of this figure is available in the online journal.)

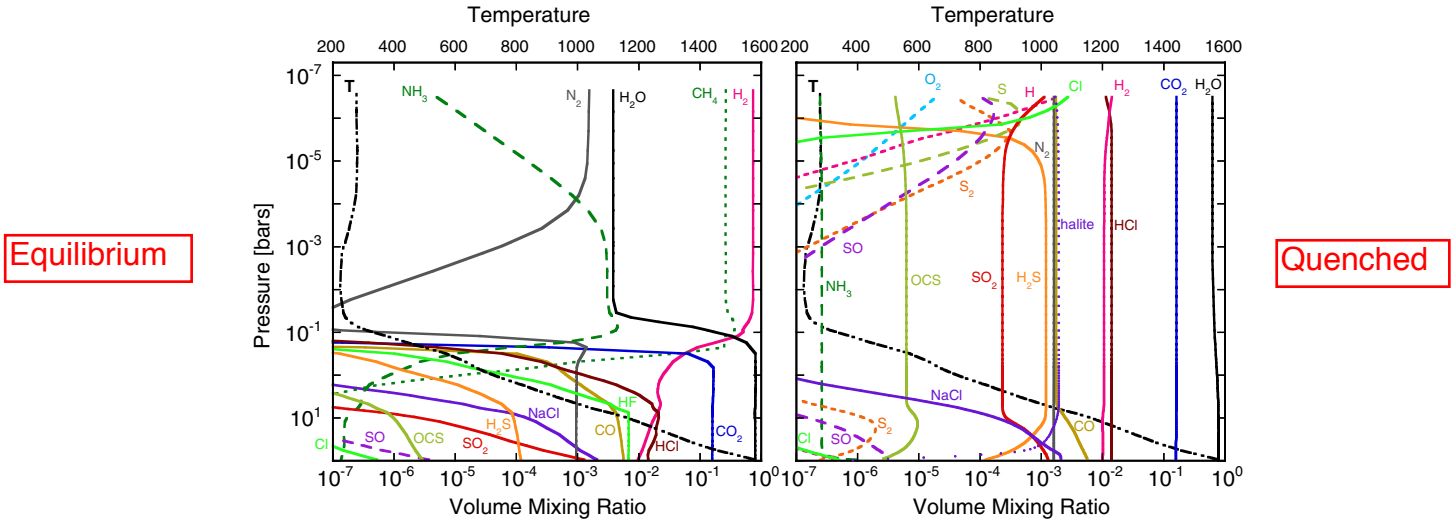

Figure 5. Same as Figure 4 for the bulk silicate earth case. Because of quenching of CH_4 and NH_3 reactions, these species are no longer important in this scenario (left panel). The atmospheric composition will resemble more closely the one for the continental crust case, dominated by water and CO_2. However, more sulfur species are produced by equilibrium chemistry in the lower atmosphere than in the continental crust case and are subsequently mixed in the higher layers.

(A color version of this figure is available in the online journal.)

are identified. As expected from the atmospheric composition, in the CC case the spectrum is dominated by H_2O and CO_2. As the surface temperature decreases, CH_4 features become more prominent, while the CO_2 features weaken. The Na I D lines at 0.59 μm are apparent at the highest $T_{\rm surf}$ and low $p_{\rm surf}$ (upper panel). The spectra of BSE models (see Figure 9) are also dominated by water absorption. However, in contrast to the CC case, the CO_2 contribution is much diminished, being only significant for the higher $T_{\rm surf}$ models, while CH_4 becomes more important, comparable to water at lower temperatures for $p_{\rm surf} = 10$ bar and especially predominant in all models for $p_{\rm surf} = 100$ bar. Interestingly, under the assumption of equilibrium chemistry, NH_3 is a significant absorber and an abundant molecule for the BSE case, with lines that become completely optically thick for most of the $p_{\rm surf} = 100$ bar models, and for low $T_{\rm surf}$ in general. The combination of H_2O, CH_4, and NH_3 lines covering most of the IR region makes these planets heavily obscured and subject to a strong greenhouse effect. For emphasis, in Figure 10 we compare directly the BSE and CC spectra shown in Figures 9 and 8. These figures clearly display the aforementioned differences between the CC and the bulk silicate earth models. They also emphasize the similarity of the two compositions for $p_{\rm surf} = 10$ bar, in which case the equilibrium chemistry for BSE does not favor significant production of CH_4 and NH_3, while the presence of larger amounts of CO_2 and SO_2 characterizes the CC spectrum.

The lower atmosphere constituents mentioned in Section 3.2 also have discernable features in the high-resolution spectra,

6.3 Chemistry of Earth's Earliest Atmosphere

B Fegley Jr., Washington University, St. Louis, MO, USA
LK Schaefer, Washington University, St. Louis, MO, USA; Present address: Harvard University, Cambridge, MA, USA

6.3.1 Introduction and Overview

In this chapter, we describe the chemistry of Earth's early atmosphere during and shortly after its formation where there is little, if any, geological record. Nevertheless, current thinking about the silicate vapor, steam, and gaseous stages of atmospheric evolution on the early Earth is potentially testable by spectroscopic observations of transiting rocky exoplanets. This assertion is supported by the rapid growth of extrasolar planetary astronomy, from the discovery of one extrasolar planet in 1995 to 838 as of the time of writing (September 2012). Over 285 transiting extrasolar planets have been discovered, and spectroscopic observations have been made for eight of them, which tentatively show one or more of the following gases in their atmospheres – H, Na, K, CO, CO_2, CH_4, H_2, H_2O, TiO, and VO (see the catalog on exoplanet.eu). Several groups are actively modeling the chemical composition (e.g., Schaefer et al., 2012) and expected spectral signatures (e.g., Marley et al., 2011) of transiting rocky exoplanets because the rapidly expanding spectroscopic capabilities will allow observational tests in the next few years. Thus, ideas about Earth's early atmosphere, which cannot be constrained by biological or geological evidence, may be indirectly constrained in the near future by astronomical observations. This point is taken up at the end of the chapter.

The nature of Earth's early atmosphere is of particular interest because it is the environment in which life originated sometime between ~4.5 and ~3.85 Ga ago (Bada, 2004). The ^{182}Hf–^{182}W and ^{146}Sm–^{142}Nd chronometers (e.g., Boyet and Carlson, 2005; Moynier et al., 2010; Yin et al., 2002) show that Earth's core formed ~30 million years, and the crust formed ~38–75 million years, respectively, after formation of the solar system 4568 Ma ago (Bouvier and Wadhwa, 2010). In other words, Earth formed ~4.54 to 4.49 Ga ago. Norman et al. (2003) derive a crystallization age of 4456 Ma ago for the earliest lunar crust, that is, 112 million years after formation of the solar system. The lunar crust must have formed after the Moon itself formed (by impact of a Mars-sized body with the early Earth). The oldest samples of continental crust are detrital zircons from Jack Hills, Australia, dating back to ~4404 Ma ago (Harrison et al., 2005; Wilde et al., 2001). The metavolcanic and metasedimentary rocks from the Nuvvuagittuq (Porpoise Cove) greenstone belt near Hudson Bay in northern Quebec have a ^{146}Sm–^{142}Nd isochron age of ~4280 Ma (O'Neil et al., 2009), which probably indicates that these rocks were derived from material extracted from Earth's mantle at that time (Arndt and Nisbet, 2012; O'Neil et al., 2009; Sleep, 2010). The oldest dated rock is the Acasta Gneiss in the Northwest Territories of Canada with an age of 4031 Ma (Bowring and Williams, 1999).

Mojzsis et al. (2001) report oxygen isotopic evidence (from the Jack Hills zircons) for liquid water on Earth's surface ~4300 Ma ago. Another oxygen isotopic study of Jack Hills zircons by Cavosie et al. (2005) suggests that liquid water existed on Earth's surface by ~4200 Ma ago and possibly as early as 4325 Ma ago. This work and other evidence led Arndt and Nisbet (2012) to conclude the Hadean Earth was more clement than previously believed.

Nonunique carbon isotopic signatures possibly indicate photoautotrophic carbon fixation in the Akilia Island banded iron formation (~3850 million years old) in Greenland (Eiler et al., 1997; Mojzsis et al., 1996). Taking these results at face value, it is concluded that Earth formed, differentiated, was struck by a giant impactor to form the Moon, and had cooled sufficiently to form continental crust within 164 million years of the formation of the solar system. Whether or not the formation of Earth and/or its differentiation was contemporaneous with lunar formation is unclear. Within another ~100–200 Ma, liquid water was present on Earth's surface. Finally, sometime in the next ~554 million years after continental crust formation, primitive life forms originated and evolved to the point where photoautotrophic activity had imprinted its carbon isotopic signature on the early Earth. The carbon isotopic signatures of photoautotrophic carbon fixation are controversial, but the available evidence indicates the development of life on Earth by ~3.8 Ga ago (e.g., see Arndt and Nisbet, 2012; Sleep et al., 2012).

As mentioned earlier, this chapter deals with the chemistry of the early terrestrial atmosphere during and shortly after formation of Earth, that is, within the period between 4540

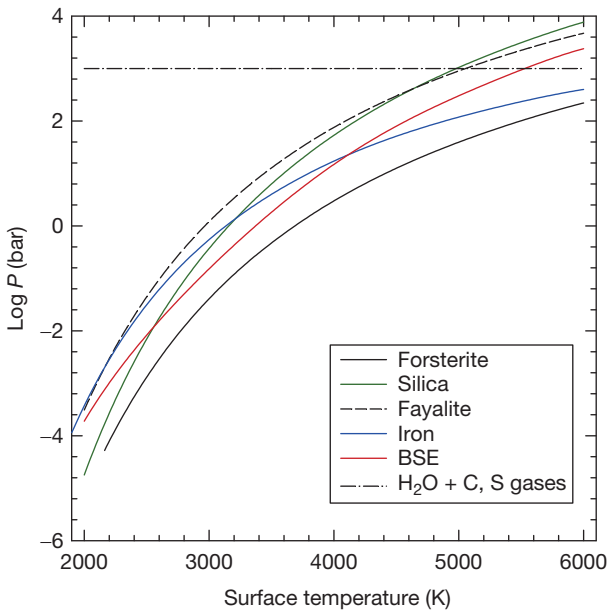

Figure 3 Temperature-dependent vapor pressures of iron metal, forsterite, fayalite, silica, and bulk silicate Earth magma are compared to the total partial pressure of $H_2O + C$, S gases corresponding to the BSE inventory of these volatiles.

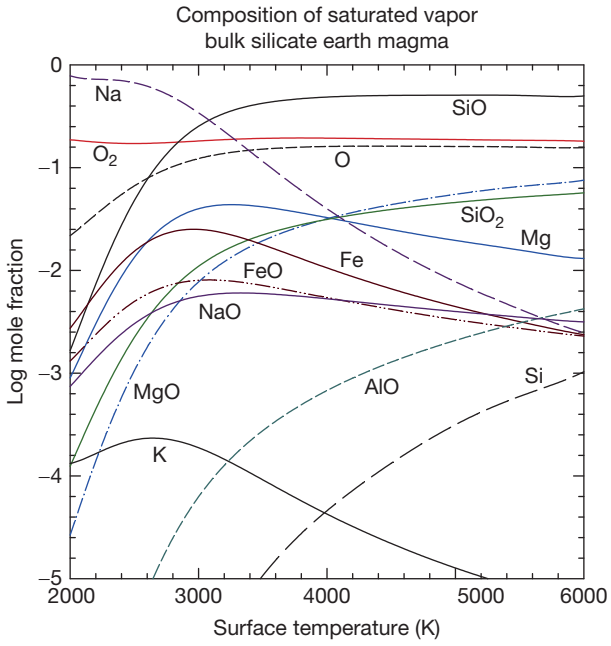

Figure 4 Temperature-dependent chemical equilibrium composition of the saturated vapor in equilibrium with bulk silicate Earth magma.

The silicate vapor is orders of magnitude more oxidizing (i.e., has a larger oxygen fugacity fO_2) than H_2-rich solar composition gas.

All other species are less abundant than Na, SiO, O_2 and O in the silicate vapor. For example, at 6000 K, the next two most abundant gases are MgO (~8%) and SiO_2 (~6%). Potassium is also volatile but monatomic K and other K-bearing gases are trace species in the vapor because of (1) the low K abundance in the BSE (Na/K atomic ratio ~17 from **Table 4**) and (2) the preferential partitioning of Na relative to K into the vapor, for example, Na/K atomic ratio ~6300 at 2000 K in **Figure 4** (also see the discussion in Schaefer and Fegley, 2004). Although Mg is about as abundant as Si in the BSE, the two major Mg-bearing gases (Mg and MgO) are much less abundant than SiO (the major Si-bearing gas) because MgO has a much lower vapor pressure than does silica; for example, at 2020 K, the saturated vapor pressures of silica and MgO are 2.4×10^{-5} and 1.2×10^{-7} bar (Farber and Srivastava, 1976a), respectively. Conversely, FeO is more volatile than MgO, and the Fe/Mg and FeO/MgO ratios in the vapor are greater than unity below ~2600 K. The opposite is true at higher temperatures. Alumina, CaO, and TiO_2 have much lower vapor pressures than the other oxides and their gases are generally much less abundant than those of the other oxides.

Knudsen effusion mass spectroscopy (KEMS) studies of solid and molten oxide vaporization are important for understanding the composition of Earth's silicate vapor atmosphere. The abundances of O and O_2 are coupled to each other via the equilibrium

$$2O(g) = O_2(g) \qquad [14]$$

Lower temperatures and higher pressures favor O_2 while higher temperatures and lower pressures favor monatomic O. Silicon monoxide SiO, O_2, and O are the major species in the saturated vapor over solid and molten silica (e.g., see Firsova and Nesmeyanov, 1960; Kazenas et al., 1985; Nagai et al., 1973; Shornikov et al., 1998; Zmbov et al., 1973). The abundances of SiO, SiO_2, which is less abundant, and Si, which is much less abundant, are coupled to one another via the equilibria

$$SiO(g) + O(g) = SiO_2(g) \qquad [15]$$

$$SiO(g) = Si(g) + O(g) \qquad [16]$$

Monatomic Mg and O_2 are the major species over solid MgO, and MgO gas is much less abundant (e.g., see Farber and Srivastava, 1976a; Kazenas et al., 1983; Porter et al., 1955). Monatomic Ca and O_2 are the major species over solid CaO, and CaO (g) is much less abundant (Farber and Srivastava, 1976b; Samoilova and Kazenas, 1995). Alumina vaporization is more complex and occurs via a combination of dissociation to the elements and the production of various Al oxides (e.g., Chervonnyi et al., 1977; Drowart et al., 1960; Farber et al., 1972; Ho and Burns, 1980). Saturated alumina vapor contains Al, O, O_2, AlO, Al_2O, Al_2O_2, and AlO_2. The O (g) partial pressure in the BSE saturated vapor is sufficiently high for AlO to be the major Al-bearing gas due to the equilibrium

$$Al(g) + O(g) = AlO(g) \qquad [17]$$

Gas phase equilibria in the silicate vapor atmosphere are rapid because of the high temperatures and pressures. This leads to chemical and isotopic equilibrium, for example, oxygen isotopic equilibrium within very short times. The elementary reactions below convert monatomic and monoxide gases of several of the major metals in the silicate vapor

Fast Kinetics

$$Si + O_2 \rightarrow SiO + O \qquad [18]$$

$$k = 1.72 \times 10^{-10} \left(\frac{T}{300}\right)^{-0.53} \exp\left(\frac{-17}{T}\right) \text{cm}^3\,\text{s}^{-1} \qquad [19]$$

$$\mathrm{Fe} + \mathrm{O_2} \rightarrow \mathrm{FeO} + \mathrm{O} \quad [20]$$

Fast Kinetics

$$k = 2.09 \times 10^{-10} \exp\left(\frac{-10\,175}{T}\right) \mathrm{cm^3\,s^{-1}} \quad [21]$$

$$\mathrm{Mg} + \mathrm{O_2} \rightarrow \mathrm{MgO} + \mathrm{O} \quad [22]$$

$$k = 4.81 \times 10^{-10} \exp\frac{-8551}{T} \mathrm{cm^3\,s^{-1}} \quad [23]$$

Similar reactions can be written for the other metals in the silicate vapor atmosphere. The bimolecular reaction rate constants are from Le Picard et al. (2001) for Si and from the NIST chemical kinetic database for Fe and Mg. The chemical lifetimes (t_{chem}, in seconds) for Si, Fe, and Mg are given by the equation

$$t_{\mathrm{chem}}(\mathrm{i}) = \frac{1}{[\mathrm{O_2}]k_\mathrm{i}} \quad [24]$$

The k_i is the reaction rate constant for the appropriate metal atom (Si, Fe, or Mg). The $[O_2]$ is the molecular number density of O_2 at any given temperature from our chemical equilibrium calculations and is given by

$$[\mathrm{O_2}] = \frac{P_{\mathrm{O_2}} N_\mathrm{A}}{RT} \quad [25]$$

In eqn [25], N_A is Avogadro's number, R is the ideal gas constant, T is temperature (K), and P_{O_2} is the O_2 partial pressure in the saturated silicate vapor.

At 2000 K, the chemical lifetimes of Si, Mg, and Fe are $10^{-3.90}$, $10^{-2.93}$, and $10^{-2.21}$ s, respectively. Reaction rates increase exponentially with temperature (as shown by eqns [19], [21], and [23]) and the chemical lifetimes of Si, Mg, and Fe are even smaller at higher temperatures. Thus, chemical and oxygen isotopic equilibrium is established very rapidly in Earth's silicate vapor atmosphere (also see Pahlevan et al., 2011 in this regard).

Chemical and oxygen isotopic equilibrium plausibly also occurs in the proto-lunar disk of molten silicate and vapor and may explain the very similar oxygen isotopic compositions of Earth and Moon (Wiechert et al., 2001). For example, at 2000 K, the O_2 molecular number density can drop by a factor of 10^6 and the chemical lifetimes given by eqn [24] are still ~1 h (Fegley et al., 2012). However, thermal escape of volatile elements and compounds from the proto-lunar disk may also have occurred. High precision Zn isotopic measurements of lunar basalts by Paniello et al. (2012) show that lunar basaltic rocks are enriched in heavier Zn isotopes and have lower Zn concentrations relative to Earth. Their results indicate evaporative Zn loss during lunar formation.

Figure 3 also shows a line giving the total pressure of H_2O, C- and S-bearing gases. This is computed assuming that all of the H_2O, carbon, and sulfur in the bulk silicate Earth (**Table 1**), which are 4.32×10^{21}, 4.03×10^{20}, and 5.00×10^{20} kg, respectively, are in the atmosphere. In this case, the pressures (P = m/g) of H_2O, C- and S-bearing gases are ~820, 80, and 96 bars, respectively, summing to ~1000 bars. (The BSE carbon abundance in Palme and O'Neill (**Chapter 3.1**) is from Zhang and Zindler (1993). If we follow Zhang and Zindler (1993) and assume that all carbon in the BSE is carbonate, the CO_2 pressure would be ~250 bars instead of ~80 bars.) All three volatiles are soluble to varying extents in silicate melts, with water and sulfur being more soluble than C-bearing gases (CO_2, CO, CH_4). Holding other variables constant, sulfur solubility depends upon oxygen fugacity and has a minimum at about the fO_2 of the Ni–NiO buffer. Sulfur dissolves as sulfide at lower fO_2 and as sulfate at higher fO_2 and has solubilities in the 100–10 000 μg g^{-1} range depending on melt composition, P, T, and fO_2 (Baker and Moretti, 2011).

Experimental studies of water and CO_2 solubility in different types of silicate melts (e.g., basaltic, feldspathic, granitic, haploandesitic, pegmatitic, rhyolitic, silicic) show that their solubility increases with increasing pressure and decreases slightly (retrograde solubility) with increasing temperature (e.g., Burnham and Jahns, 1962; Goranson, 1931; Hamilton et al., 1964 , Holtz et al. 1995, Karsten et al., 1982; Mysen and Wheeler, 2000; Schmidt and Behrens, 2008; Yamashita, 1999). However, the temperature coefficients are small, for example, ~0.1 to 0.3 wt% H_2O per 100 K increase, and have been measured over fairly small temperature intervals of 300 K or less at temperatures at or below 1300 °C (1573 K). A molecular dynamics simulation of CO_2 solubility in silicate melts covers the 1200–2000 °C (1473–2273 K) range, and predicts decreasing solubility with increasing temperature (Guillot and Sator, 2011). But there are no experimental data for H_2O, CO_2, or sulfur solubility in molten peridotite or other silicate melts at the temperatures expected on Earth's surface after the Moon-forming impact.

H_2O and CO_2 solubility in silicate melts was modeled using the VolatileCalc program of Newman and Lowenstern (2002). The calculated solubilities of H_2O (820 bar) and CO_2 (80 bar) at 2000 K are 3.06 wt% and 36 μg g^{-1}, respectively. VolatileCalc predicted prograde solubility for water with a temperature coefficient of 0.029 wt% per 100° and a constant solubility for CO_2. Sulfur solubility was not modeled because of the complex dependence on T, P, fO_2, and melt composition.

The line for these volatiles in **Figure 3** may thus be an upper limit, but a comparison with the vapor pressure curves of the molten silicates is instructive. **Figure 3** shows that the atmospheric partial pressure of water and other volatiles is larger than the saturated vapor pressure of the BSE magma until ~5525 K. If 90% of H_2O, C, and S are dissolved in the magma, 100 bars of volatiles remain in the atmosphere and the magma must be at ~4630 K for its vapor pressure to be comparable. Equality of the molten silicate vapor pressure and volatile partial pressure occurs at 3925 K if 99% of H_2O, C, and S are dissolved in the magma, and 10 bars of volatiles remain. Even if 99.9% of H_2O, C, and S are dissolved in the magma and only 0.1% remains in the atmosphere ($P_{volatile}$ = 1 bar), the BSE magma must be at 3352 K to have the same pressure. In other words, the silicate vapor atmosphere may be mainly steam, C-, and S-bearing gases even if most of the water, C, and S in the BSE are dissolved in the super-liquidus BSE magma. At present, the partitioning of volatile elements between the magma and silicate vapor cannot be computed with certainty and new experimental data on the solubility of water, C-, and S-bearing gases in silicate melts, especially molten peridotite, at superliquidus temperatures are required. This is important because the most abundant gases (Na, O, O_2) in the saturated silicate vapor are infrared-inactive. Silicon monoxide has strong IR bands at 4 μm (first overtone) and 8 μm (fundamental) and lines throughout the millimeter region. By analogy to CO_2,

SiO_2 (with a mole fraction >0.1% for $T > 2300$ K) may be a good greenhouse gas. However, the most efficient greenhouse gases in the silicate vapor atmosphere may be H_2O, CO_2, and SO_2.

Fegley and Schaefer (2006) modeled condensate cloud formation in Earth's silicate vapor atmosphere assuming an adiabatic temperature gradient and a surface temperature of 2000 K. As **Figure 3** shows, the silicate vapor is dominantly Na, O_2, O with smaller amounts of Fe, SiO, FeO, Mg, and other gases at this temperature. Their predicted cloud condensation sequence as a function of altitude in the silicate vapor atmosphere is Mg_2SiO_4 (1955 K, 4.5 km), liquid $CaAl_2Si_2O_8$ (1931 K, 7 km), liquid $CaSiO_3$ (1896 K, 9.5 km), cristobalite (1870 K, 13 km), Fe_3O_4 (1817 K, 18 km), rutile (1602 K, 40 km), and Na_2O (1169 K, 82 km). The Na_2O cloud was the most massive, followed by the cristobalite, magnetite, and forsterite cloud layers. The liquid anorthite, liquid wollastonite, and rutile layers were thin hazes because their abundances were severely limited by the small amounts of Ca, Al, and Ti in the silicate vapor at 2000 K. Monatomic K remained in the gas and never condensed from the atmosphere. A different condensate cloud sequence with liquid oxide and silicate clouds was predicted for a hotter atmosphere (5000 K surface T). This is consistent with the temperature-dependent composition of the silicate vapor (**Figure 3**).

In principle, the results of Fegley and Schaefer (2006) can be checked by spectroscopic observations of hot rocky exoplanets. The three known examples as of the time of writing (September 2012) are CoRoT-7b (substellar surface $T \sim 2474$ K, Léger et al., 2011), Kepler-10b (substellar surface $T \sim 3038$ K, Léger et al., 2011), and 55 Cnc e (substellar surface $T \sim 2800$ K, Winn et al., 2011). All three planets are probably tidally locked with the same side always facing the parent star. The average surface temperatures are lower than the substellar temperatures and are ~1810 K (CoRoT-7b), ~1833 K (Kepler-10b), and ~1967 K (55 Cnc e).

The only published spectroscopic observations of hot rocky exoplanets to date are those of Guenther et al. (2011) who searched for gaseous Ca, Ca^+, CaO, and Na in the exosphere of CoRoT-7b. They did not detect any of these gases. However, all Ca and Na are predicted to condense into clouds below an altitude of 100 km and to be absent in the exospheres of hot rocky exoplanets (Fegley and Schaefer, 2006; Schaefer and Fegley, 2009; Schaefer et al., 2012).

Fegley and Schaefer (2006) did not model the photochemistry of the silicate vapor atmosphere but some general statements can be made. Nemtchinov et al. (1997) give linear absorption coefficients for H chondrite vapor in the visible and IR ranges. At one bar pressure, the optical absorption coefficients are 0.01–10 cm^{-1} and the IR absorption coefficients are 10^{-6}–1 cm^{-1}. Much of the opacity is due to Fe-bearing gases. Iron is more abundant in H chondrites than in the BSE (16.7 wt% Fe metal vs. 8.18% FeO) and the opacity of BSE vapor may be lower. Silicon monoxide absorbs light shortward of 300 nm (Matveev, 1986; Podmoshenskii et al., 1968; Vorypaev, 1981)

$$SiO + h\nu \rightarrow Si + O \quad \lambda < 300\ nm \qquad [26]$$

However, reaction [18] may rapidly regenerate SiO gas. Solar UV photolysis of O_2 ($\lambda < 240$ nm) may produce monatomic oxygen and ozone via the Chapman cycle:

$$\text{Photolysis of } O_2 \quad O_2 + h\nu \rightarrow O + O\ (\lambda = 180 - 240\ nm) \qquad [27]$$

$$\text{Ozone production} \quad O + O_2 + M \rightarrow O_3 + M \qquad [28]$$

$$\text{Ozone photolysis} \quad O_3 + h\nu \rightarrow O(^1D) + O_2\ (\lambda = 200 - 300\ nm) \qquad [29]$$

$$\text{Oxygen production} \quad O + O + M \rightarrow O_2 + M \qquad [30]$$

$$\text{Ozone destruction} \quad O + O_3 \rightarrow O_2 + O_2 \qquad [31]$$

$$\text{Net reaction} \quad O + O_3 \rightarrow O_2 + O_2 \qquad [32]$$

The M in reactions [28] and [30] is a third body that can be any other gas. But O_3 thermal decomposition may reverse the outcome of these photochemical reactions. Water vapor ($\lambda < 212$ nm), CO_2 ($\lambda < 227.5$ nm), and SO_2 ($\lambda < 210$ nm), and their thermal dissociation products (OH, CO, SO) may also be photolyzed by the enhanced UV flux of the early Sun. Qualitatively, the situation is similar to that for the hot gas giant exoplanets called 'roasters' such as HD 209458 and HD 189733b. These planets are very close to their primary stars (e.g., HD 209458b is 0.05 AU from its primary and receives 10 000 times the solar flux at Jupiter) where UV photons are being dumped into their hot tropospheres. There is a critical atmospheric level for each species where the thermochemical (t_{thermo}) and photochemical (t_{photo}) lifetimes are equal, below which $t_{thermo} < t_{photo}$ in the thermochemical zone and above which $t_{thermo} > t_{photo}$ in the photochemical zone (see section 5 of Visscher et al., 2006; Moses et al., 2011). The difference between Earth's silicate atmosphere and the 'roaster' planets is that Earth is O_2-rich and oxidizing while the roasters are H_2-rich and reducing. A combined photochemical–thermochemical model is necessary to delineate the photochemically and thermochemically active zones of Earth's silicate vapor atmosphere. Again, in principle, spectroscopic observations of hot rocky exoplanets can indirectly constrain chemistry on the hot early Earth – something that was not even dreamed of a few years ago.

6.3.6 Steam Atmosphere

Arrhenius et al. (1974) were probably the first to propose that Earth had a steam atmosphere early in its history. They calculated that heating during accretion of Earth should release water from the accreting material and lead to formation of a H_2O-bearing atmosphere and oceans after cooling. Radiative cooling calculations indicate that cooling took ~2.5 Ma (Sleep et al., 2001). Shortly after the work of Arrhenius et al. (1974), Ahrens and colleagues experimentally studied impact degassing of the Murchison CM2 carbonaceous chondrite, carbonates, and hydrous minerals (e.g., Lange and Ahrens, 1982a,b, 1986; Tyburczy and Ahrens, 1985, 1987, 1988; Tyburczy et al., 1986a,b). Due in large part to their work, it is generally accepted that conversion of at least some of the kinetic energy of accreted planetesimals into heat led to impact degassing of volatiles during the accretion of Earth. Water and CO_2 were the major species released by impact degassing of the materials Ahrens and colleagues studied; thus, impact-generated atmospheres have historically been called steam atmospheres (e.g., Abe and Matsui, 1985; Lange and Ahrens, 1982a). Models of

Earth's steam atmosphere and magma ocean were developed by Abe and Matsui in a series of pioneering papers (Abe and Matsui, 1985, 1987; Matsui and Abe, 1986). More recent work on the terrestrial magma ocean is described by Abe (1997), Abe et al. (2000), and Elkins-Tanton (2012), and that on the steam atmosphere is discussed by Zahnle et al. (1988, 2007, 2010) and Sleep et al. (2001).

Figure 5 shows the chemical equilibrium composition of the H_2O, C, and S gases at a constant total pressure of 1000 bars in Earth's steam atmosphere. This pressure corresponds to the complete BSE inventories of water, C, and S. As mentioned earlier, neither the solubility of water, CO_2, and S in molten peridotite nor the temperature dependence of their solubilities in peridotite and silicate melts are well known. But if they have retrograde solubility with constant temperature coefficients of ~0.1 wt% per 100 K, virtually no volatiles would be in super-liquidus temperature melts.

Figure 5 is plausibly an upper limit to the pressures of these gases in Earth's steam atmosphere. Zahnle et al. (1988) modeled steam atmospheres with 100–300 bars water, but did not consider CO_2 or sulfur. They correctly noted that "a fully self-consistent treatment would need to consider the partitioning of carbon between CO_2, CO, CH_4, and graphite and the solubilities of these species in the melt." Pawley et al. (1992) found that CO was insoluble in MORB basaltic melt at 1200 °C and 500–1500 bar pressures, but we are unaware of CH_4 solubility data for silicate melts. Again, more experimental data on volatile solubilities in super-liquidus silicate melts appear to be needed.

Figure 5 illustrates several interesting points. Water vapor remains the major gas in the steam atmosphere until ~5700 K where OH becomes more abundant. At 6000 K, OH and H have almost identical abundances. At temperatures below ~3600 K, H_2O, CO_2, and SO_2 are the three most abundant gases. Above this point, OH becomes more important and displaces SO_2, CO_2, and, finally, H_2O as a major gas. Dioxygen and H_2 are produced by thermal dissociation of water, but the fO_2 is only ~0.1 log unit larger than in a pure steam atmosphere because O_2 produced by thermal dissociation of water inhibits O_2 production by thermal dissociation of CO_2, and SO_2 to some extent. The production of H and H_2 reduces some sulfur to HS and H_2S, but both remain minor species. The abundances of CH_x gases (e.g., CH, CH_2, CH_3, CH_4) are even smaller and are not shown on the graph.

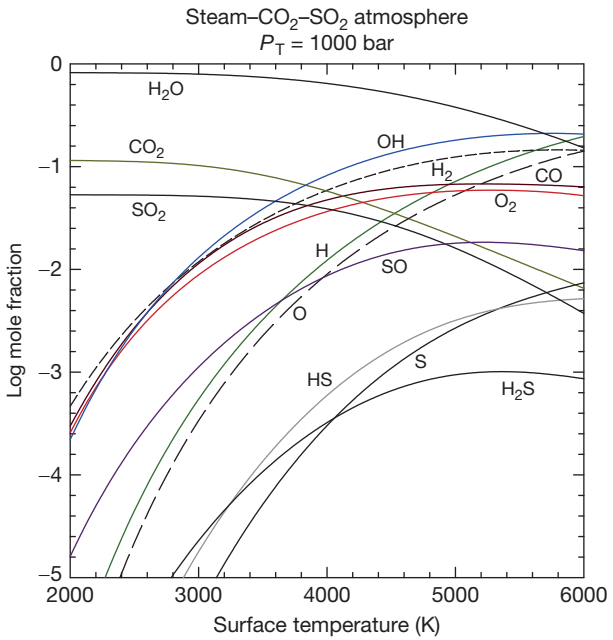

Figure 5 Temperature-dependent chemical equilibrium composition of Earth's steam atmosphere at 1000 bar total pressure.

"Steam" Atmosphere Thermochemistry

The steam atmosphere, like the silicate atmosphere, is significantly more oxidizing (i.e., has a larger oxygen fugacity fO_2) than the H_2-rich solar nebula and as a result, easily oxidized elements (e.g., Cr, Mo, W as gaseous oxides and H_2CrO_4, H_2MoO_4, H_2WO_4 gases, Fe as $Fe(OH)_2$ vapor, B as H_3BO_3 (g), Si as H_4SiO_4 (g), V as gaseous oxides) may partition between the magma ocean and steam atmosphere. All of these elements occur in sublimate minerals that condensed out of terrestrial (steam-rich) volcanic gases at volcanic or fumarolic vents (see Table 1 in Brackett et al., 1995).

Sleep et al. (2001) used PVT data on the NaCl–water system (Bischoff, 1991) and an analogy with chemistry at modern mid-ocean ridges to discuss the chemistry and water–rock interactions in the steam atmosphere. Depending on the pressure, the PVT data indicate that either halite (at 754 K, 300 bar) or a NaCl-rich brine forms. Sleep et al. (2001) also note that Cl-bearing amphiboles form at temperatures below ~1023 K in modern mid-ocean ridge axes. Schaefer et al. (2012) found that halite condenses at 1550 K, 100 bar in their modeling of the steam atmosphere produced by heating the bulk silicate Earth. Schaefer et al. (2012) did not have thermodynamic data for endmember Cl-bearing amphiboles or micas for their calculations, but Cl may substitute for the F- and OH-bearing micas and amphiboles, which do form. For example, at 100 bar total pressure, it is found that fluorphlogopite is stable below 1350 K and pargasite is stable below 1000 K in the steam atmosphere produced by heating the BSE. Thus, there is qualitative agreement between the steam atmosphere models of Schaefer et al. (2012) and the mid-ocean ridge analogy of Sleep et al. (2001).

As noted above, the steam atmosphere lasted for ~2.5 Ma. After most of the steam rained out to form the oceans, Earth's atmosphere was plausibly dominated by 'traditional' volatiles. Using **Figure 5** as a guide, it may be inferred that the major gases were mainly CO_2 with smaller amounts of SO_2, H_2, H_2S, and H_2O. The water vapor partial pressure was limited by its saturation vapor pressure and may have been ~50% of the saturated value as in Earth's troposphere today. Molecular N_2 was also probably abundant because NH_3 is so thermally unstable that it could not exist in an early steam atmosphere (see **Table 5**). Sleep and Zahnle (2001) showed that most of the atmospheric CO_2 (~250 bar in their work) could be lost by carbonization and subduction of rocks such as basalts or ultramafics. The timescale for loss of a CO_2-rich atmosphere is 10–100 Ma and depends on the details of their models.

However, it is also possible that the 'traditional' volatiles left after collapse of the steam atmosphere were more reducing. Schaefer and Fegley (2010) showed that the 'steam' atmosphere produced on either an ordinary chondritic (H, L, LL) or enstatite chondritic (EH, EL) early Earth was H_2O-poor and

important factor determining the redox state of the outgassed atmospheres.

We conclude by returning to a point mentioned in the introduction, namely, how spectroscopic observations of rocky exoplanets may provide indirect constraints on ideas about Earth's early atmosphere. As noted earlier, as of the time of writing (September 2012), there are three rocky exoplanets with sufficiently high surface temperatures to support silicate vapor atmospheres. These planets are CoRoT-7b ($T \sim 2474$ K, $1.58 R_E$, $7.42 M_E$, $\rho \sim 10.4$ g cm^{-3}), Kepler-10b ($T \sim 3038$ K, $1.42 R_E$, $4.54 M_E$, $\rho \sim 8.7$ g cm^{-3}), and 55 Cnc e ($T \sim 2800$ K, $2.0–2.1 R_E$, $8.0–8.6 M_E$, $\rho \sim 5.0–5.9$ g cm^{-3}), whose substellar temperatures are listed (see earlier discussion). The key gases to observe on these planets are SiO and H_2O. The presence of SiO gas proves the existence of a silicate vapor atmosphere and the presence (or absence) of H_2O shows whether or not the planet is volatile depleted. Carter et al. (2012) recently reported the discovery of the rocky exoplanet Kepler-36b. The radius, mass, and density of Kepler-36b are $\sim 1.49 R_E$, $\sim 4.45 M_E$, and ~ 7.5 g cm^{-3}, respectively. It has a calculated surface temperature of ~ 980 K, which is hot enough to support a steam atmosphere. The key point to be observed in this case (or of any other similar rocky exoplanets) is whether or not abundant H_2O and CO_2 or H_2 and CO are present because these pairs of gases provide information on the oxidation state of the planet. In the ideal case, a series of rocky exoplanets with surface temperatures ranging from ~ 300 to 2500 K could be observed spectroscopically. At present, this lies in the future. But the future may show that the answers to understanding Earth's early atmosphere lie not only in the rock record but also in astronomical observations of worlds beyond our solar system.

Acknowledgments

This work was supported by NASA cooperative agreement NNX09AG69A with the NASA Ames Research Center and by grants from the NSF Astronomy Program. We dedicate this chapter to the memory of our friend Al Cameron, who originally got B.F. interested in the chemical consequences of the Moon-forming impact. We thank David Fike, Mark Marley, and Fred Moynier for their comments, Jim Tyburczy and Kevin Zahnle for their reviews of the manuscript, and James Farquhar for his extraordinary patience while waiting for this chapter to be completed.

References

Abe Y (1997) Thermal and chemical evolution of the terrestrial magma ocean. *Physics of the Earth and Planetary Interiors* 100: 27–39.

Abe Y (2011) Protoatmospheres and surface environment of protoplanets. *Earth, Moon, and Planets* 108: 9–14.

Abe Y and Matsui T (1985) The formation of an impact-generated H_2O atmosphere and its implications for the early thermal history of the Earth. *Proceedings of the 15th Lunar and Planetary Science Conference*, pp. C545–C559.

Abe Y and Matsui T (1987) Evolution of an impact-generated H_2O–CO_2 atmosphere and formation of a hot proto-ocean on Earth. *Lunar and Planetary Sci Conference* 18: 1–2.

Abe Y, Ohtani T, Okuchi K, Righter K, and Drake M (2000) Water in the early Earth. In: Canup R and Righter K (eds.) *Origin of the Earth and Moon*, pp. 413–433. Tucson, AZ: University of Arizona Press.

Abelson PH (1966) Chemical events on the primitive Earth. *Proceedings of the National Academy of Sciences of the United States of America* 55: 1365–1372.

Ackermann RJ, Rauh EG, Thorn RJ, and Cannon MC (1963) A thermodynamic study of the thorium – Oxygen system at high temperatures. *Journal of Physical Chemistry* 67: 762–769.

Allegre CJ, Poirier J-P, Humler E, and Hofmann AW (1995) The chemical composition of the Earth. *Earth and Planetary Science Letters* 134: 515–526.

Arndt NT and Nisbet EG (2012) Processes on the young Earth and the habitats of early life. *Annual Review of Earth and Planetary Sciences* 40: 521–549.

Arrhenius G, De BR, and Alfvén H (1974) Origin of the ocean. In: Goldberg ED (ed.) *The Sea*, vol. 5, pp. 839–861. New York: Wiley-Interscience.

Aston FW (1924a) Atomic species and their abundance on the Earth. *Nature* 113: 393–395.

Aston FW (1924b) The rarity of the inert gases on the Earth. *Nature* 114: 786.

Bada JL (2004) How life began on Earth: A status report. *Earth and Planetary Science Letters* 226: 1–15.

Baker DR and Moretti R (2011) Modeling the solubility of sulfur in magmas: A 50-year old geochemical challenge. *Reviews in Mineralogy and Geochemistry* 73: 167–213.

Ballentine CJ and Holland G (2008) What CO_2 well gases tell us about the origin of noble gases in the mantle and their relationship to the atmosphere. *Philosophical Transactions of the Royal Society of London* 366A: 4183–4203.

Barshay SS (1981) *Combined Condensation – Accretion Models of the Terrestrial Planets*. PhD Thesis, MIT, Cambridge, MA.

Bernal JD (1949) The physical basis of life. *Proceedings of the Physical Society* 62A: 537–558.

Bischoff JL (1991) Densities of liquids and vapors in boiling NaCl–H_2O solutions: A PVTX summary from 300° to 500° C. *American Journal of Science* 291: 309–338.

Bouvier A and Wadhwa M (2010) The age of the solar system redefined by the oldest Pb–Pb age of a meteoritic inclusion. *Nature Geoscience* 3: 637–641.

Bowring SA and Williams IS (1999) Priscoan (4.00–4.03 Ga) orthogneisses from northwestern Canada. *Contributions to Mineralogy and Petrology* 134: 3–16.

Boyet M and Carlson RW (2005) ^{142}Nd evidence for early (>4.53 Ga) global differentiation of the silicate Earth. *Science* 309: 576–581.

Brackett RA, Fegley B Jr., and Arvidson RE (1995) Volatile transport on Venus and implications for surface geochemistry and geology. *Journal of Geophysical Research* 100(E1): 1553–1563.

Brandes JA, Boctor NZ, Cody GD, Cooper BA, Hazen RM, and Yoder HS (1998) Abiotic nitrogen reduction on the early Earth. *Nature* 395: 365–367.

Brock DS and Schrobilgen GJ (2011) Synthesis of the missing oxide of xenon, XeO_2, and its implications for Earth's missing xenon. *Journal of the American Chemical Society* 133: 6265–6269.

Brown H (1949) Rare gases and the formation of the Earth's atmosphere. In: Kuiper GP (ed.) *The Atmospheres of the Earth and Planets*, pp. 260–268. Chicago: University of Chicago Press.

Bukvic D (1979) *Outgassing of Chondritic Planets*. M.S. Thesis, MIT, Cambridge, MA.

Burnham CW and Jahns RH (1962) A method for determining the solubility of water in silicate melts. *American Journal of Science* 260: 721–745.

Caffee MW, Hudson GB, Velsko C, et al. (1999) Primordial noble gases from the Earth's mantle: Identification of a primitive volatile component. *Science* 285: 2115–2118.

Cameron AGW and Ward WR (1976) The origin of the Moon. *7th Lunar Science Conference*, pp. 120–122.

Canup RM (2008) Accretion of the Earth. *Philosophical Transactions of the Royal Society of London* 366A: 4061–4075.

Carter JA, Agol E, Chaplin WJ, et al. (2012) Kepler-36: A pair of planets with neighboring orbits and dissimilar densities. *Science* 337: 556–559.

Cavosie AJ, Valley JW, Wilde SA, and E.I.M.F. (2005) Magmatic δ^{18}O in 4400–3900 Ma detrital zircons: A record of the alteration of recycling of crust in the early Archean. *Earth and Planetary Science Letters* 235: 663–681.

Centolanzi FJ and Chapman DR (1966) Vapor pressure of tektite glass and its bearing on tektite trajectories determined from aerodynamic analysis. *Journal of Geophysical Research* 71: 1735–1749.

Chase MW (1998) *NIST-JANAF Thermochemical Tables*, 4th edn. *Journal of Physical and Chemical Reference Data* (Monograph), vol. 9. Washington, DC/Woodbury, NY: The American Chemical Society/The American Institute of Physics.

Chervonnyi AD, Piven VA, Kashireninov OE, and Manelis GB (1977) Mass spectrometric investigations of gas-phase equilibria over Al_2O_3 at high temperatures. *High Temperature Science* 9: 99–108.

Chou CL (1978) Fractionation of siderophile elements in the Earth's upper mantle. *Proceedings of the 9th Lunar and Planetary Science Conference*, pp. 219–230.

January 2014

Exoplanetary Time Machine to the Early Earth

Professor Bruce Fegley, Washington University in St. Louis

We cannot travel back in time to see events unfolding on the early Earth. There is no direct geological or biological evidence from the earliest Earth for us to study, as the Earth's surface is always evolving. But there must be rocky exoplanets that are at the various analogous stages that the Earth went through over time – in fact some of these rocky exoplanets are already known at present. Thus, we can utilize observations of some of the 1,000+ exoplanets discovered to date and those of yet to be discovered exoplanets as a "Time Machine to the Early Earth" to test long held ideas and characterize key aspects of the early Earth. In this way, we can investigate many fundamental questions about the early Earth including, complex chemistry during its accretion, the existence (if any) of silicate and steam atmospheres prior to formation of reducing CH_4, NH_3, H_2; or perhaps oxidizing CO_2, N_2 atmospheres, pre-biotic chemistry in the early atmosphere and ocean, and possibly the origin of life itself.

One may ask can we really hope to find rocky exoplanets that mimic the different stages of Earth's 4.5 billion years long evolution? The answer is a resounding yes. The compound annual growth (CAG) of exoplanet discoveries is ~ 44% between the detection of the first exoplanet around a main sequence star in 1995 and the 1056 exoplanets known now. Even with lower CAG, it is certain that many more rocky cousins of the early Earth will be found (e.g., only 14.4% CAG is needed to double the number of known exoplanets in 5 years).

We need observations of other worlds to fill the gaps in our knowledge of what occurred on the early Earth. But, to maximize information return, we need to know what to look for. We have already modeled atmospheric composition and emergent spectra of selected rocky exoplanets that might be akin to early Earth conditions, and determined characteristic atmospheric tracers. For example, exoplanets such as CoRoT-7b, Kepler-10b, and Kepler-78b are hot enough to possibly have magma oceans and silicate vapor atmospheres. They are a potential source of information about the situation on early Earth after the Giant

Moon-Forming Impact. Kepler-36b and other exoplanets like it may provide information about the putative steam atmosphere on the early Earth.

The proof of whether such atmospheres exist on many other Earth-like planets will come through future observations, anticipated in 2018 with JWST and beyond, and TESS in 2017. But we will be ready to place the new observations into a timeline that could map and test the conditions during important eras of Earth's evolution. Whatever path the early Earth took during its infancy, each stage will have characteristic signatures, and these signatures are what the early Earth analogs among the exoplanets will show.

We will model the atmospheric chemistry and the emergent spectra in order to define the detectability of relevant spectral features with JWST and other instruments. Our published past work shows we are capable to benchmark the abilities that future observatories will need to have to detect particular characteristic molecules at particular wavelengths.

We combine chemistry from our proprietary chemistry codes and atmospheric modeling. I have the relevant expertise though my 30+ years of modeling chemistry of the solar nebula, other protoplanetary disks, and planetary atmospheres. The emergent spectral modeling done in the past by Prof. Fortney – in our group for this proposal – also demonstrates his capability to carry out this plan. One result of our prior work on chemistry of protoplanetary disks is that we know many exoplanetary systems can provide information relevant to our own world. Unless stellar metallicity is 1.5-2 dex (~ 32 – 100) times smaller than solar – unusual for stars with rocky exoplanets – chondritic relative abundances of rocky elements are preserved and bulk planetary compositions like Earth can be formed. The volatile to rocky element abundances of exoplanets can be modeled with Earth as the nominal model and looking at variations from this using the volatile inventory of different terrestrial planets and chondritic meteorites as a guide.

My proposed work addresses several research topics relevant to questions 1 – 4 and complements work by several investigators (e.g., Dworkin, Kaltenegger, Sasselov among others). I hope to show that we can indeed use the Exoplanetary Time Machine to travel back to the early Earth and see what transpired so long ago.

Comparison of K behaviors in MAGMA model (revised 20140314) and MELTS model

- Yu et al. (2003) evaporation experiments
- Richter et al. (2011) evaporation experiments
- BSE evaporation modeling

MAGMA revised 20140314

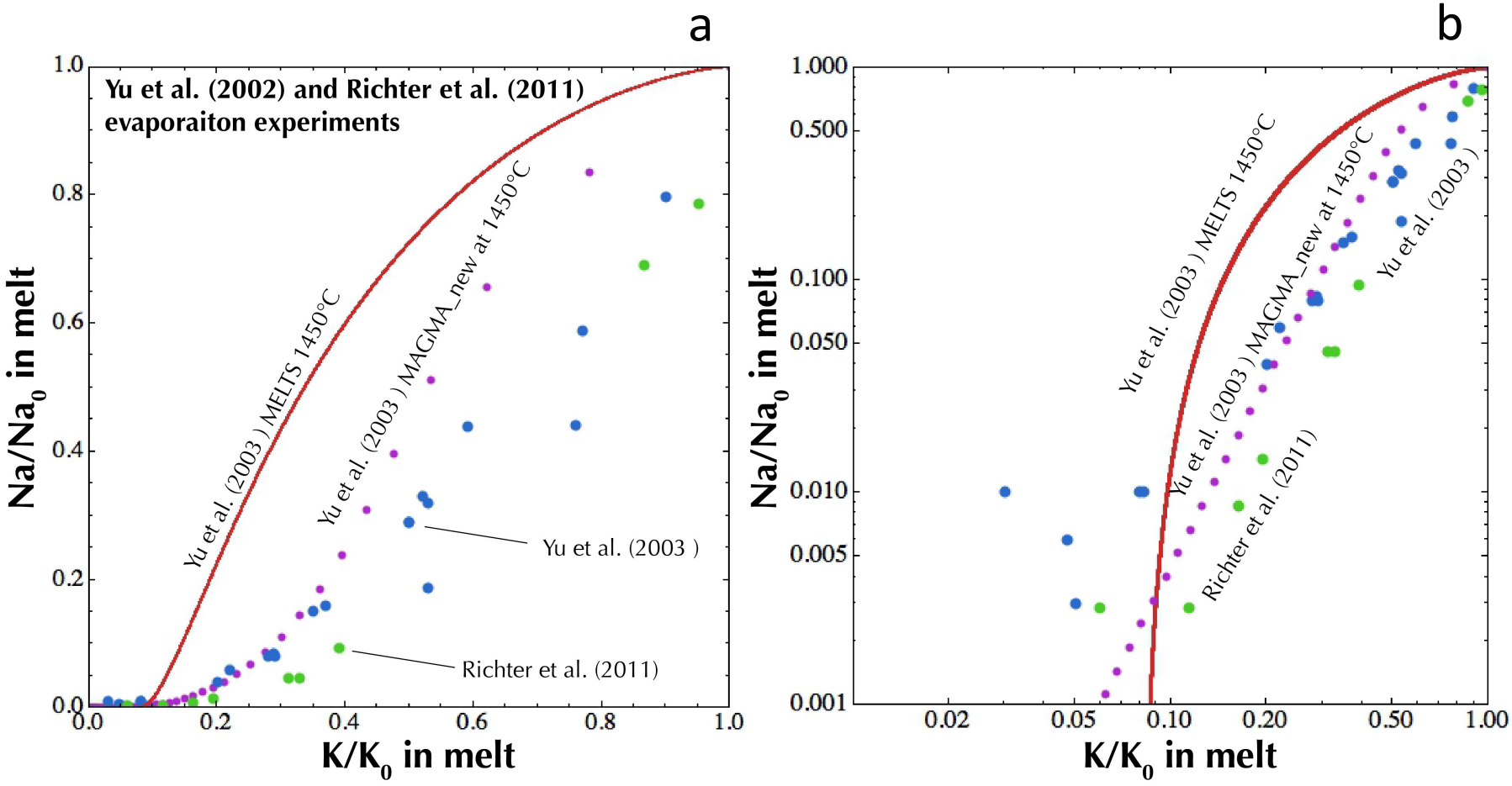

Fig. 2

Vapor pressure of K gas species and activity of K components in the melt

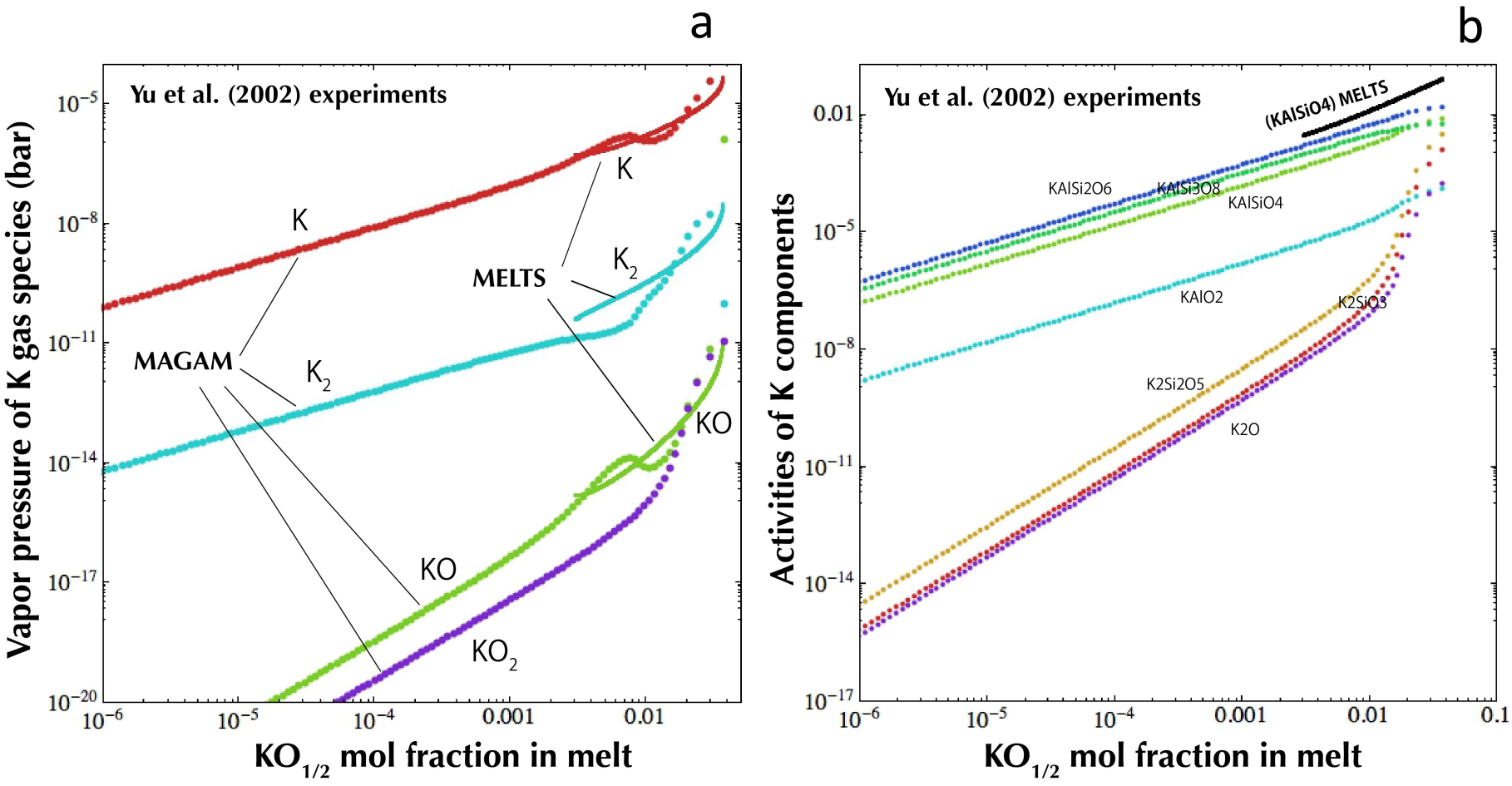

Fig. 2

MAGMA revised 20140314

Composition of saturated vapor
Bulk silicate Earth magma
New Na, K values - Holland & Powell 2011
liquid alkali aluminosilicate data

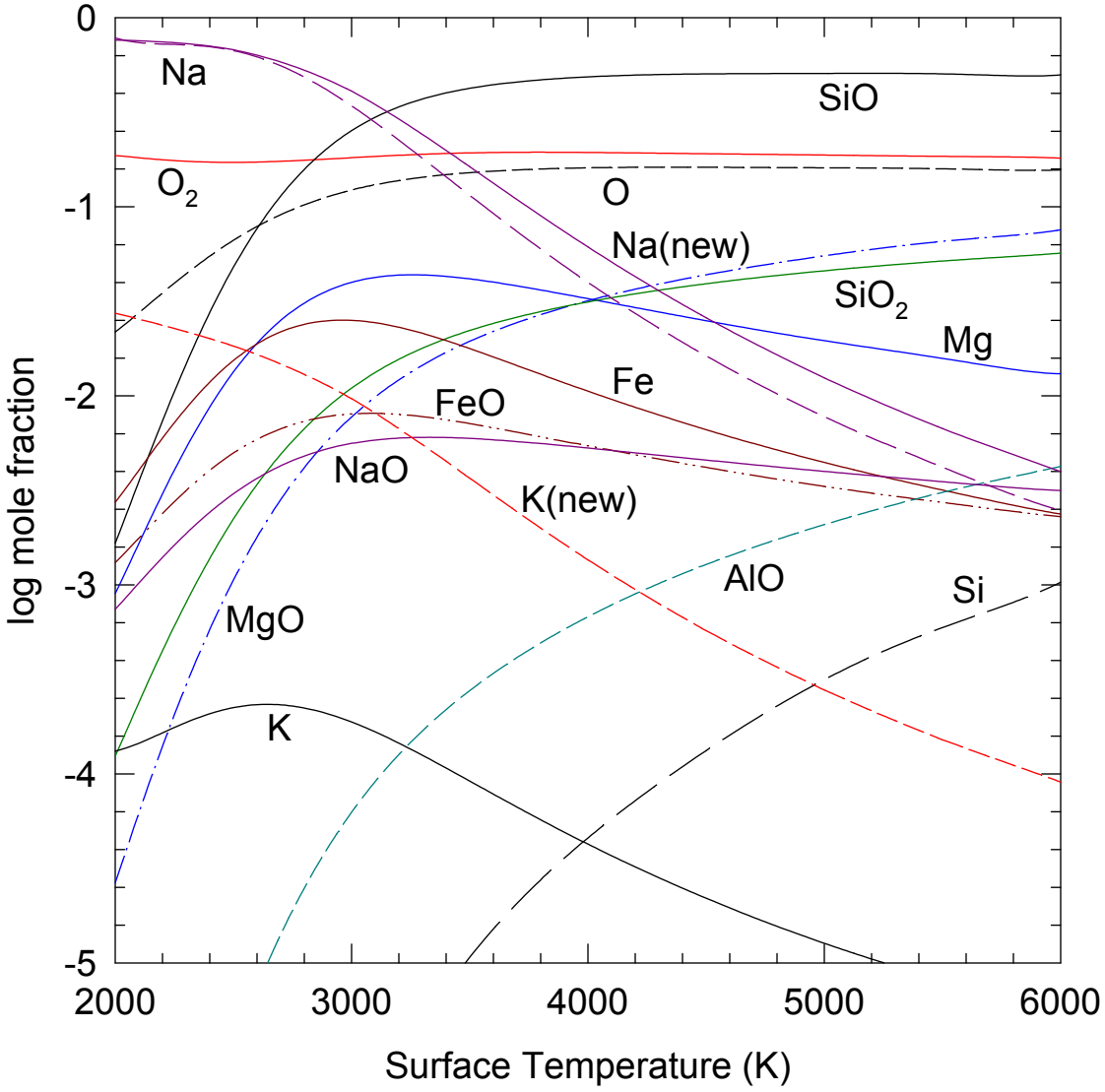

Solubility of Lava Planets in Steam Atmospheres

Bruce Fegley, Jr.

Planetary Chemistry Laboratory,

Department of Earth & Planetary Sciences and

McDonnell Center for the Space Sciences,

Washington University, St. Louis, MO 63130 USA

bfegley@wustl.edu

Introduction. All major rock-forming cations (e.g., Si, Mg, Fe, Ca, Al, Na, K, Ti) and many minor and trace elements (e.g., Li, Rb, Cs; Be, Sr, Ba; Y; REE; Zr; V; Cr, Mo, W; B, Ga, In, Tl; U, Pu) form volatile hydroxide and/or oxyhydroxide gases [1,2]. Chemical equilibrium models predict rocky elements partition into atmospheres as hydroxide gases in larger amounts than expected from their volatility over molten lavas at the high temperatures expected for steam atmospheres on the early Earth and hot rocky exoplanets [3,4].

I discuss some calculations for Si chemistry of lava planets with steam atmospheres. The results predict spectroscopically observable gases on these planets, are useful for modeling steam atmosphere chemistry on the early Earth, and for understanding chemistry of water in hot, silicate melt – vapor disks formed by giant impacts such as the hypothesized Moon-forming impact.

Silica-saturated melts are the simplest case.

References

[1] JANAF Tables

[2] Meschter, P.J. et al. (2013) Annu. Rev. Mat. Res. 43, 559-588.

[3] Schaefer, L., Lodders, K. & Fegley, B., Jr. (2012) Astrophys. J. 755:41 (16 pp) 2012 August 10, doi:10.1088/0004-637X/755/1/41

[4] Fegley, B., Jr. & Schaefer, L. (2014) Chemistry of Earth's Early Atmosphere, Chapter 6.3 in Treatise on Geochemistry, 2nd ed. http://dx.doi.org/10.1016/B978-0-08-095975-7.01303-6

[5] Centolanzi, F.J. & Chapman, D. R. (1966) J. Geophys. Res. 71(6), 1735-1749.

[6] Melosh, H. J. (2007) Meteoritics Planet. Sci. 42, 2079-2098.

[7] Schaefer, L., & Fegley, B., Jr. (2004) Icarus 169, 216-241.

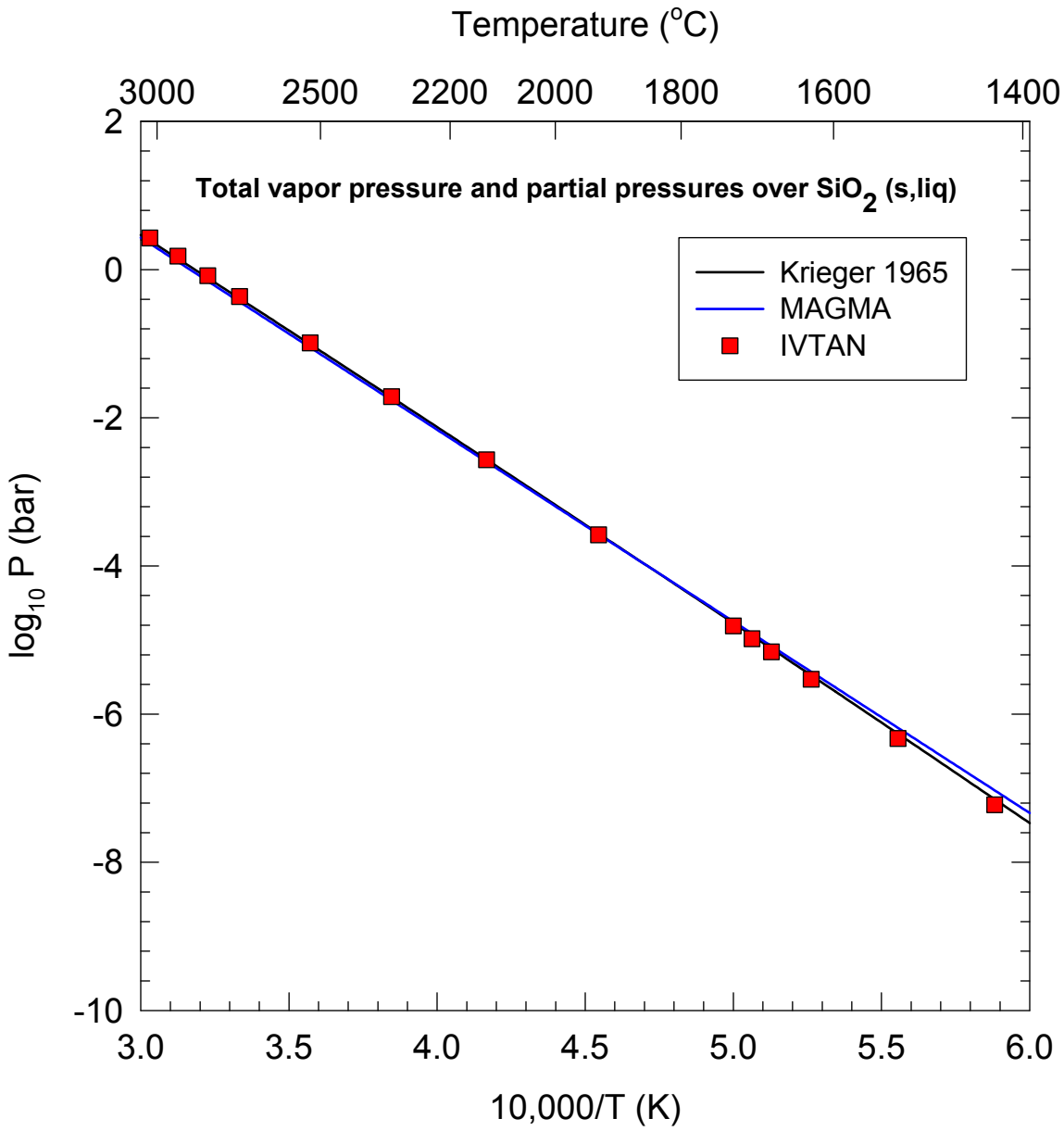

SiO2vap.SPW - IVTAN code

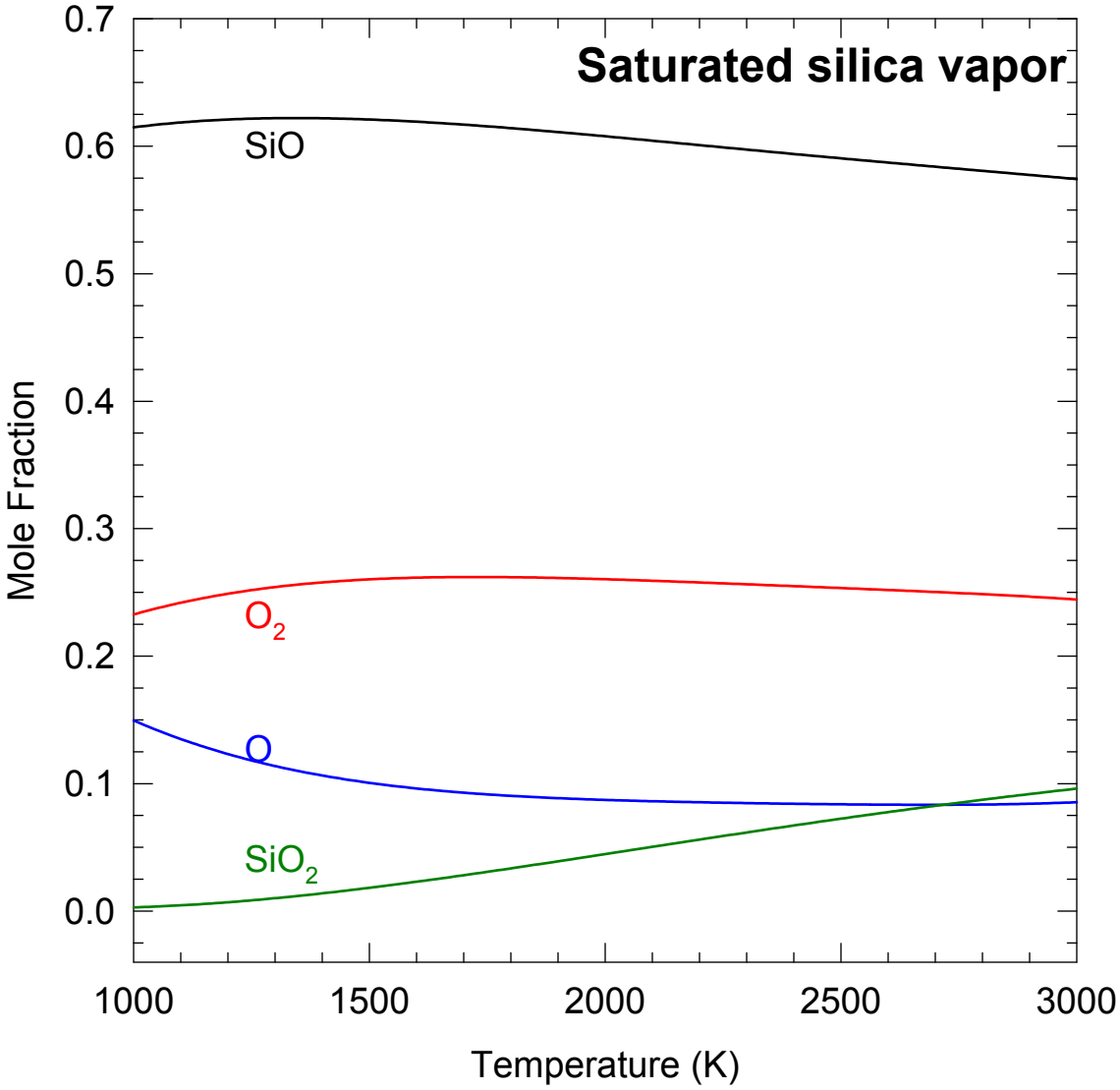

SiO2vap.SPW - IVTAN code

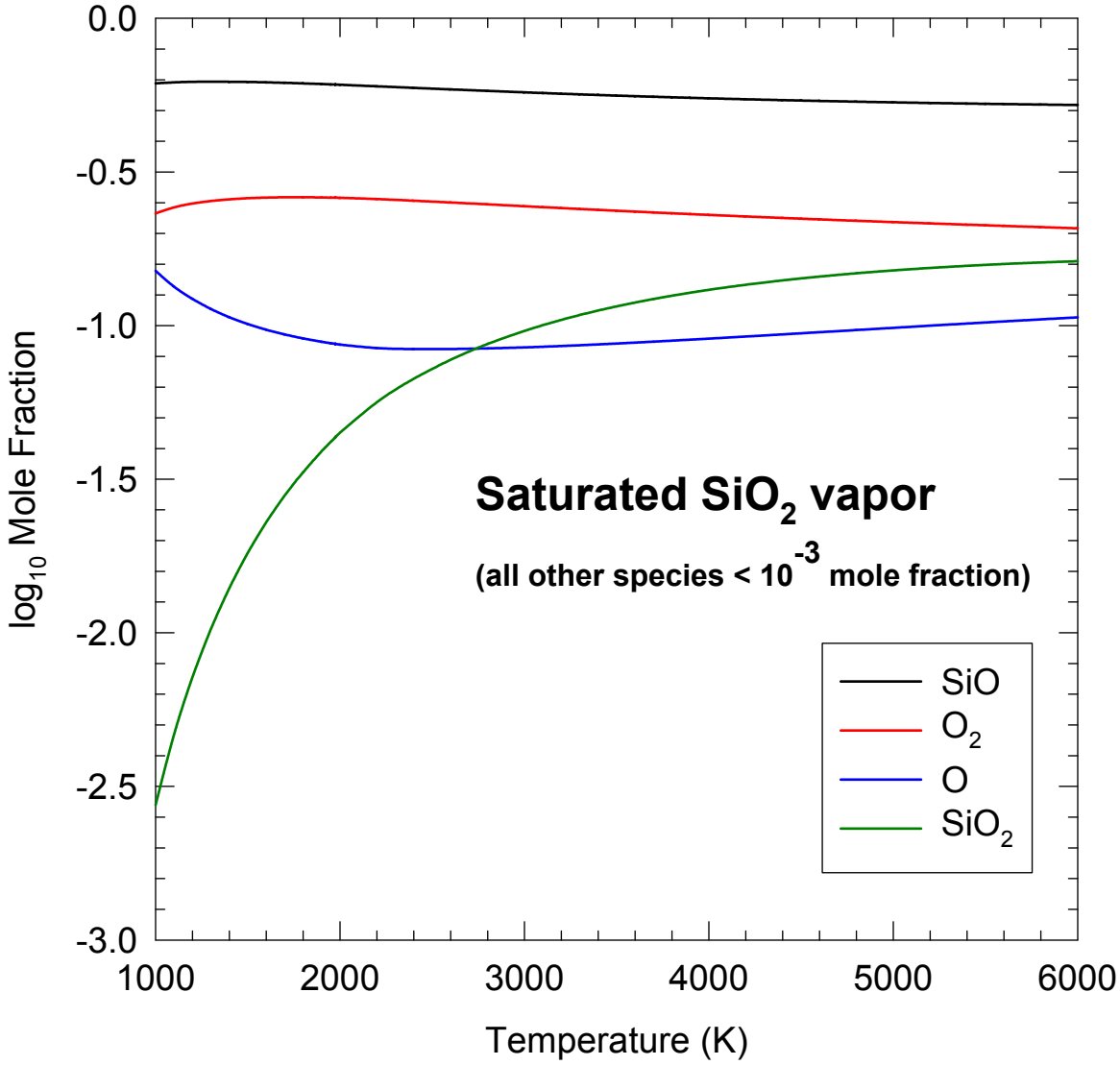

SiO2vap.SPW - IVTAN code

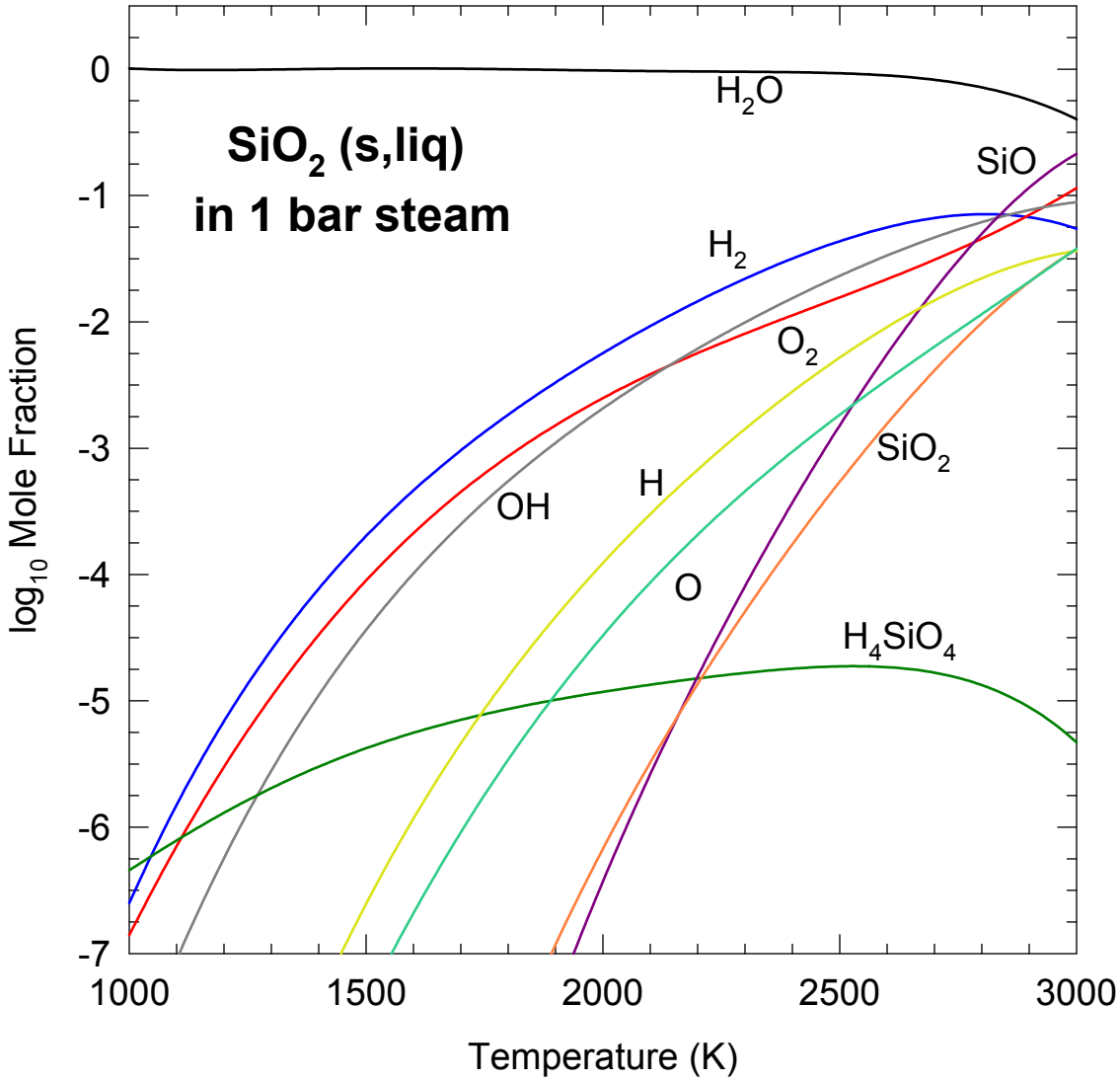
SiO2 (s,liq)
in 1 bar steam
H2O
SiO
H2
O2
SiO2
H
OH
O
H4SiO4
log10 Mole Fraction
Temperature (K)
0
-1
-2
-3
-4
-5
-6
-7
1000
1500
2000
2500
3000

wetSiO2.spw

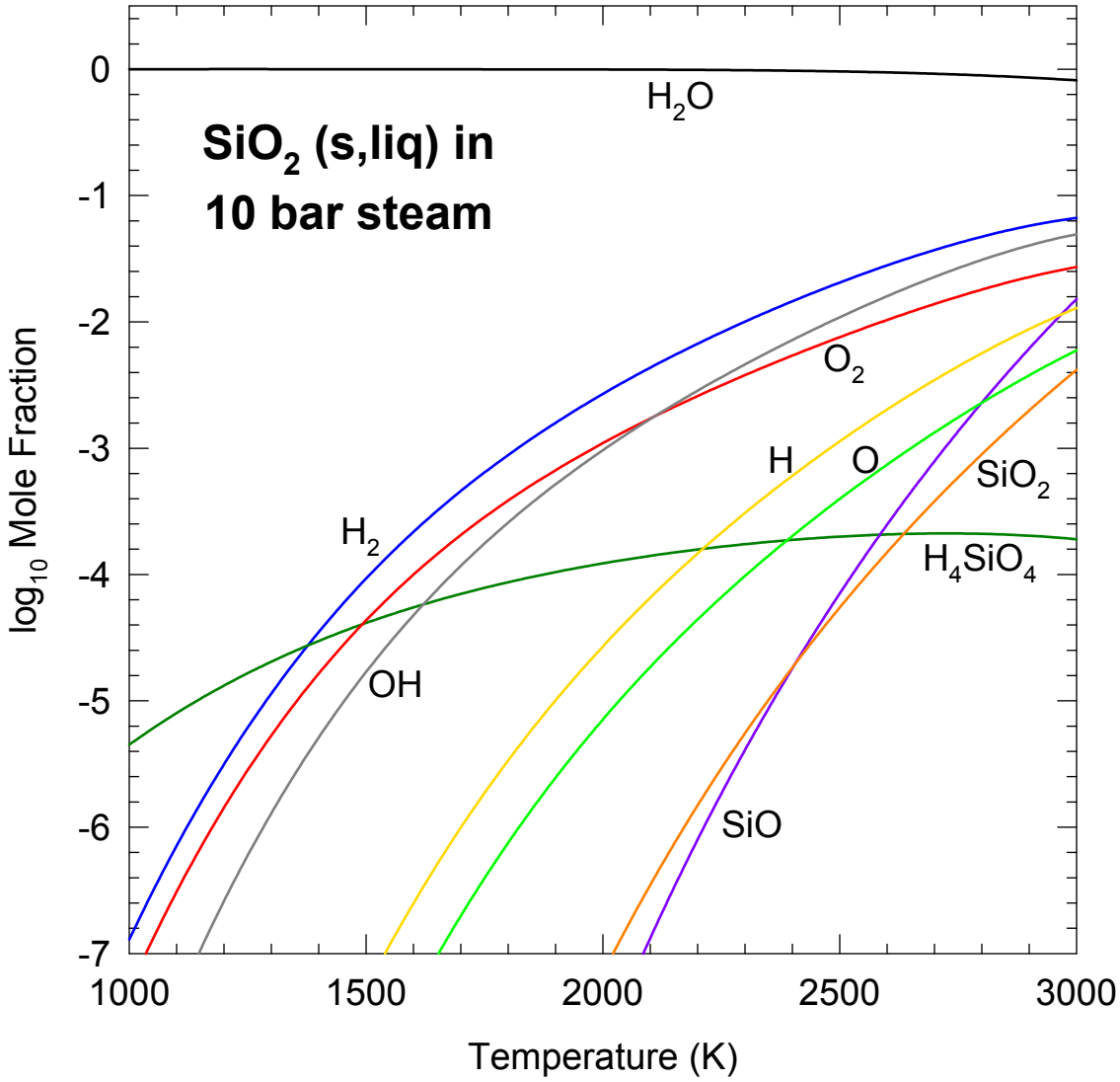

wetSiO22.spw

log f_{O_2} in a pure steam atmosphere

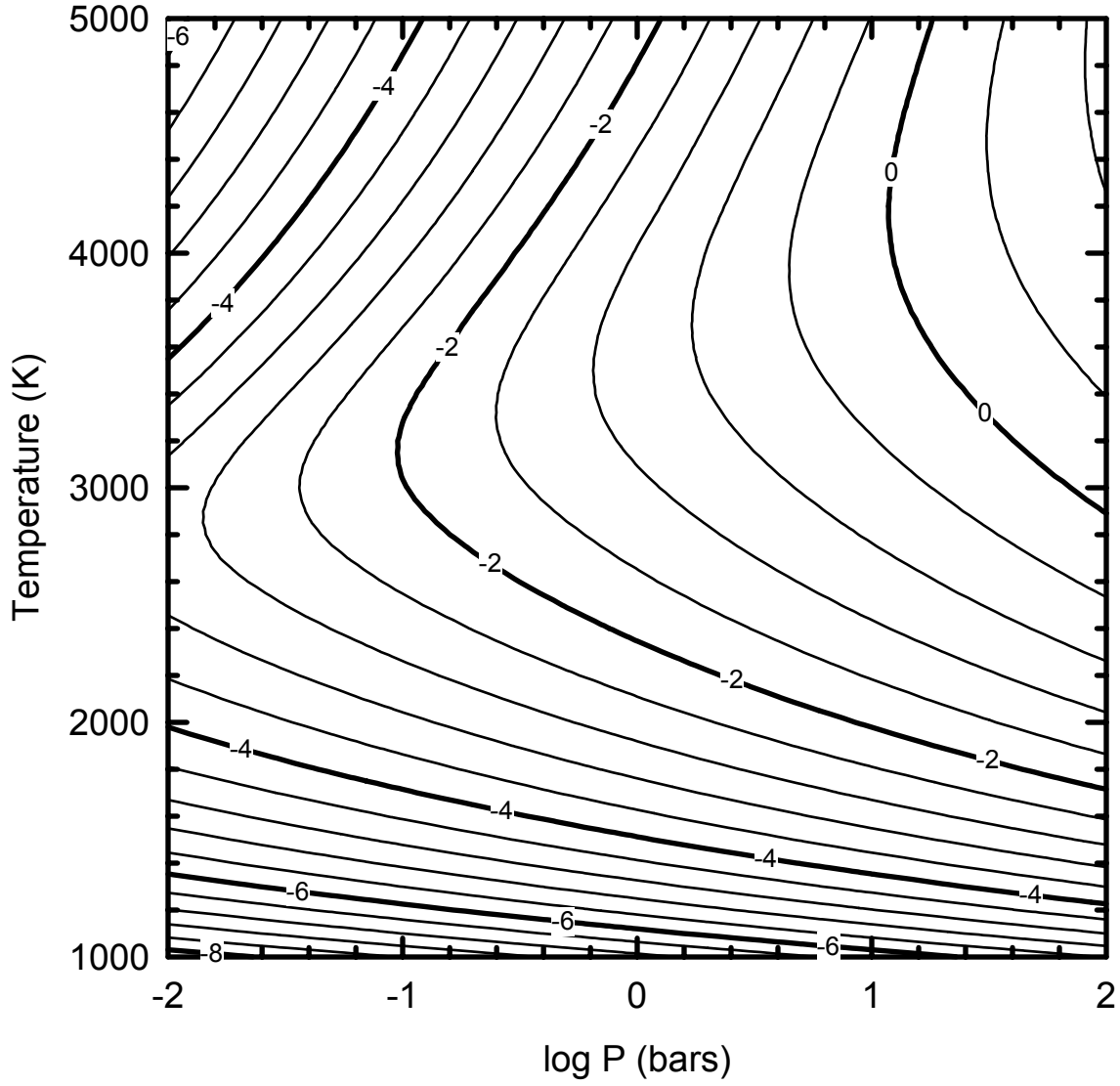

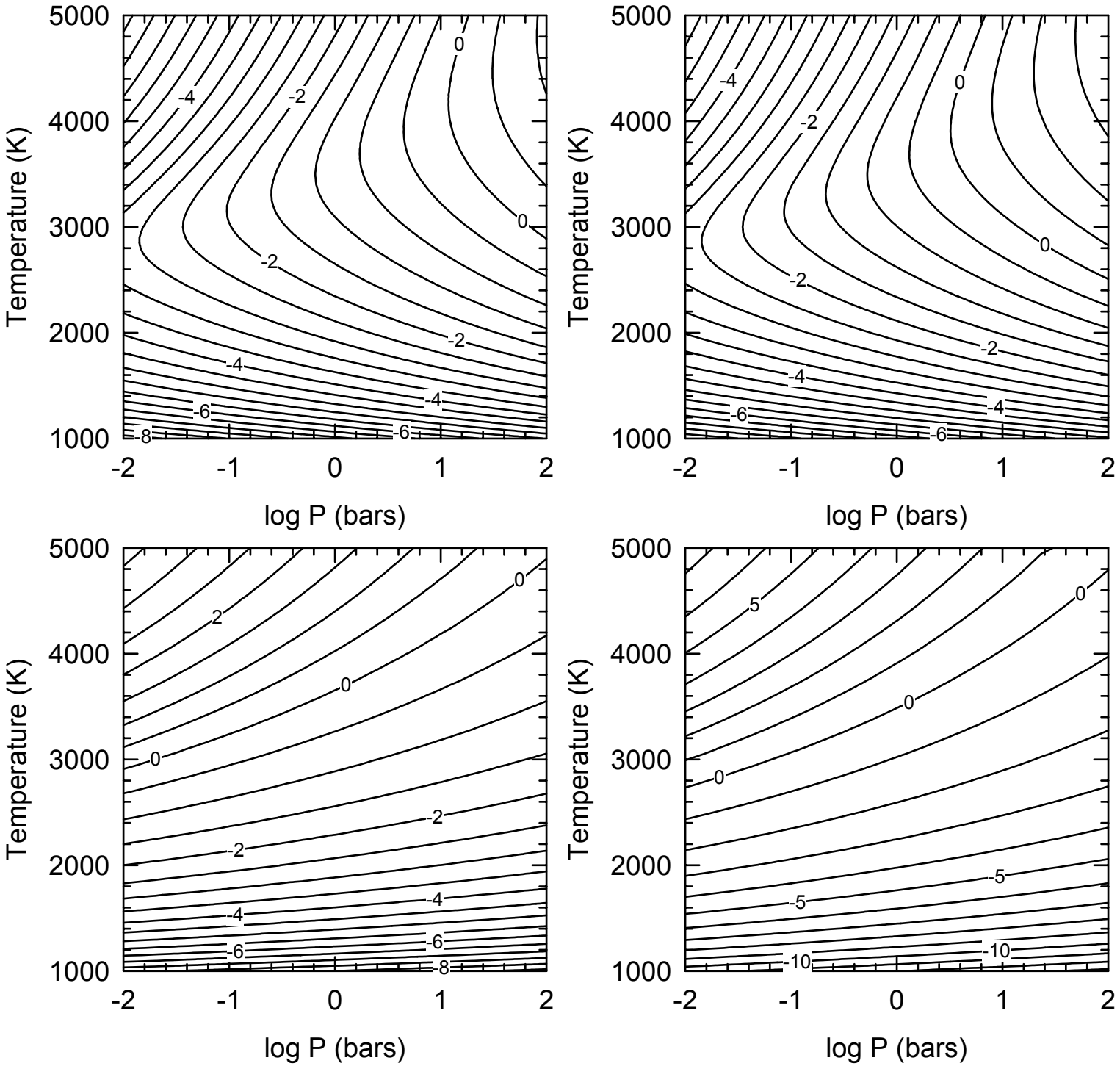

Figure 1. Chemical equilibrium calculations for a pure steam atmosphere.
top left - log fO_2 (bar) contours, top right - log fH_2 (bar) contours,
bottom left - log OH/H_2O molar ratio, bottom right - log H/H_2O molar ratio.

Chemical equilibrium models of the redox state of Earth's earliest atmosphere

LAURA SCHAEFER[1] AND BRUCE FEGLEY, JR.[2]

[1]Harvard University, Department of Astronomy, Cambridge, MA 02138, lschaefer@cfa.harvard.edu

[2]Washington Univeristy, Earth & Planetary Sciences Department, 1 Brookings Dr., St. Louis, MO 63130

The Earth's present day atmosphere is the product of secondary outgassing of accreted volatiles and impact degassing of planetesimals. The Earth can be modeled as a mixture of primitive materials, such as carbonaceous (C), ordinary (O), or enstatite (E) chondrites. In previous work, we calculated the composition of the outgassed atmospheres of large planetesimals and the early Earth [1,2] and the impact-degassed atmospheres [3] of these primitive materials. We found that outgassing of O-chondrites produces a reducing atmosphere rich in CH_4 (see Fig. 1) [1,2]. In contrast, impact degassing of C-chondrites produces oxidized, water- & CO_2-rich atmospheres, whereas impact degassing of O- & E-chondrites produced H_2-rich atmospheres with large amounts of CO and water vapor [3]. Here, we will further explore the oxidation states of these atmospheres. We will explore the effect of a range of temperatures and pressures on the results.

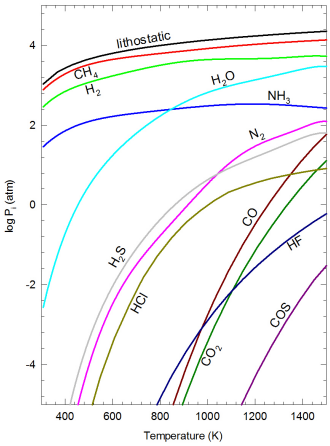

Fig. 1. Outgassed atmosphere from an Earth-like planet composed of ordinary chondritic material. From [4]

[1] Schaefer, L. and Fegley, B., Jr. (2005) *BAAS,* **37**, 67. [2] Schaefer, L. and Fegley, B., Jr. (2007). *Icarus*, **186**, 462-483. [3] Schaefer, L. and Fegley, B. Jr. (2010) *Icarus*, **208**, 438-448. [4] Fegley, B., Jr., and L. Schaefer, L. (2013) *Treatise on Geochemistry*, 2nd ed, Ch. 6.3.

Oxidation state of meteorite atmospheres

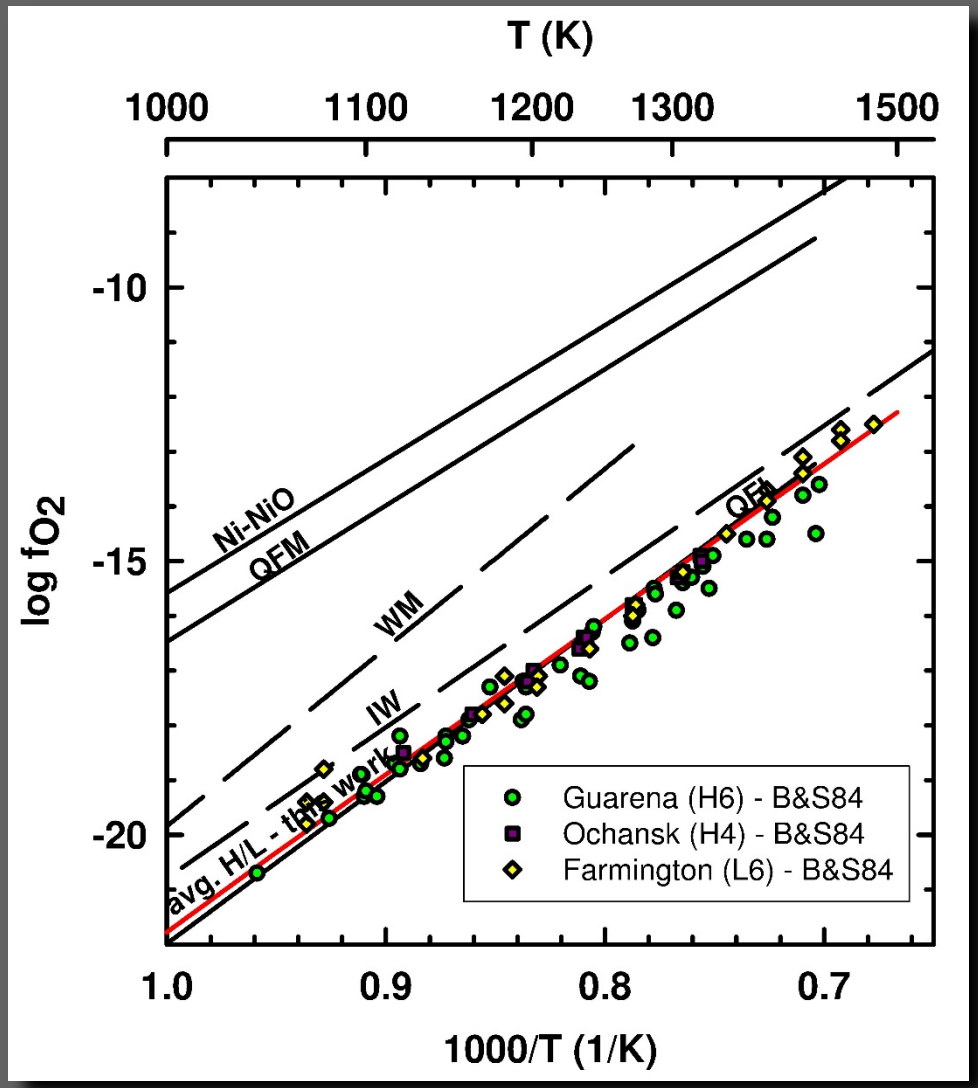

Oxygen fugacity does not depend on total pressure

haefer & Fegley (2007)

Oxidation state of meteorite atmospheres

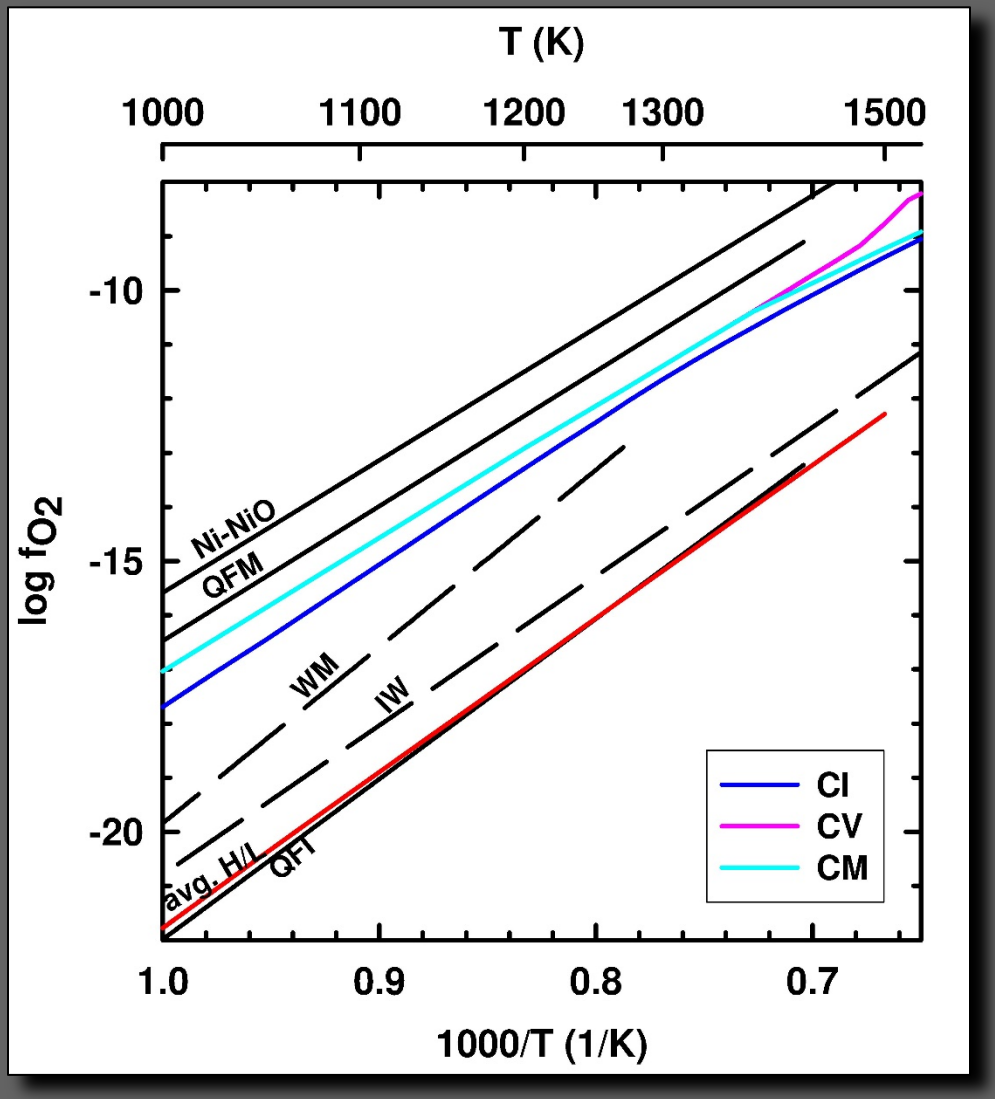

Carbonaceous chondrite have higher fO2 than ordinary chondrites.

CI chondrites have lower fO2 than CM & CV chondrites.

Oxidation state of meteorite atmospheres

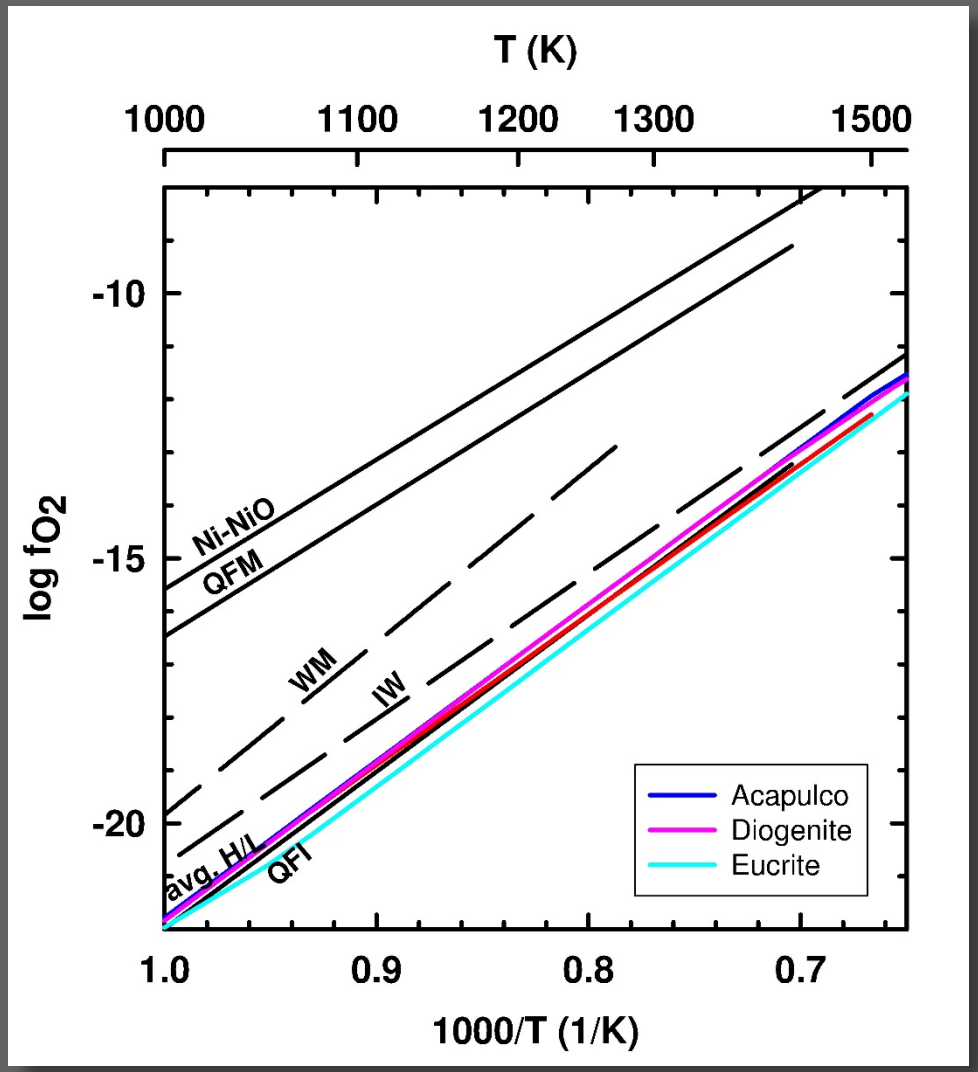

Achondrites have similar
fO2 to ordinary/enstatite
chondrites.

10% CV + 90% H mixture

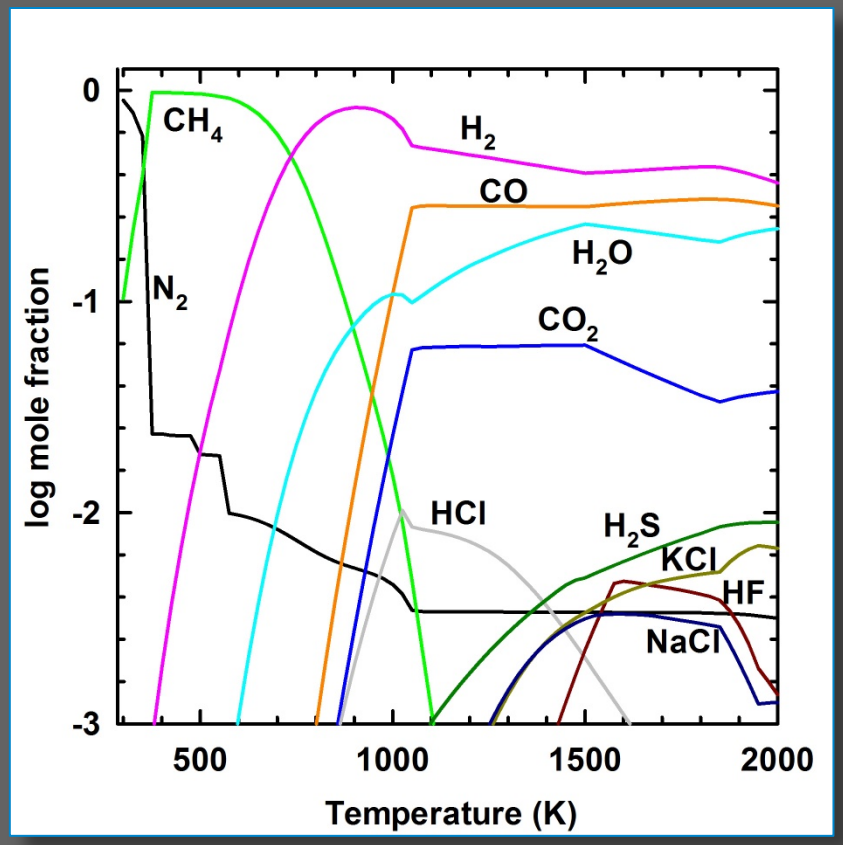

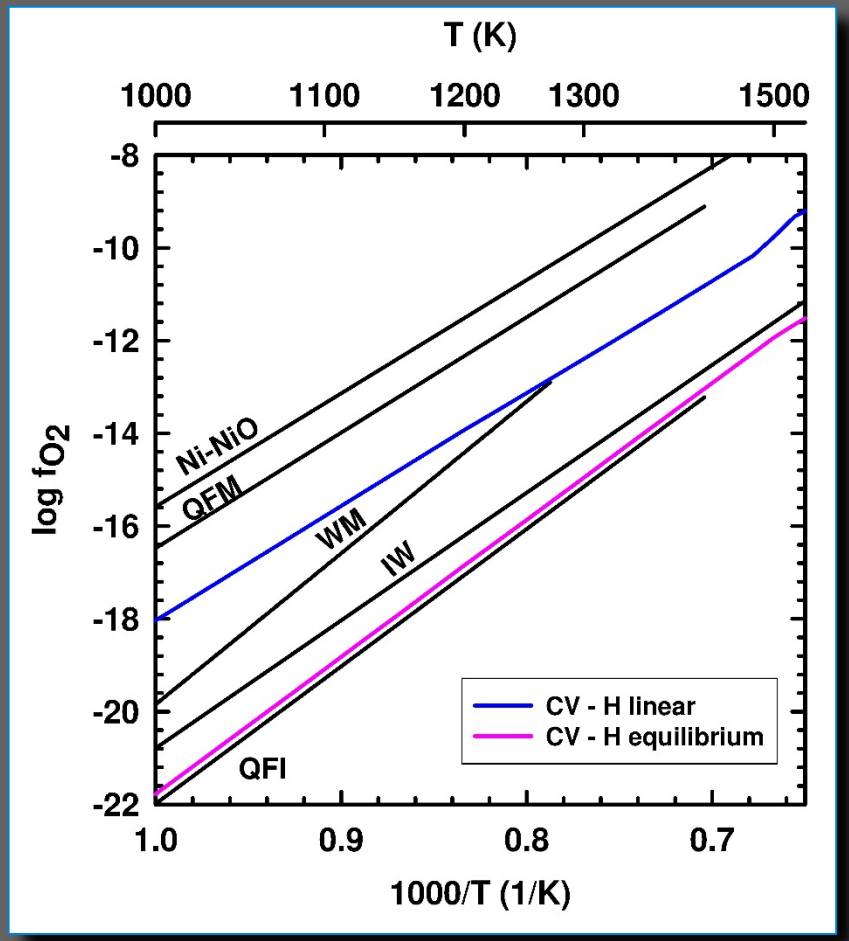

CI – CV – H mixtures (1500 K, 1 bar)

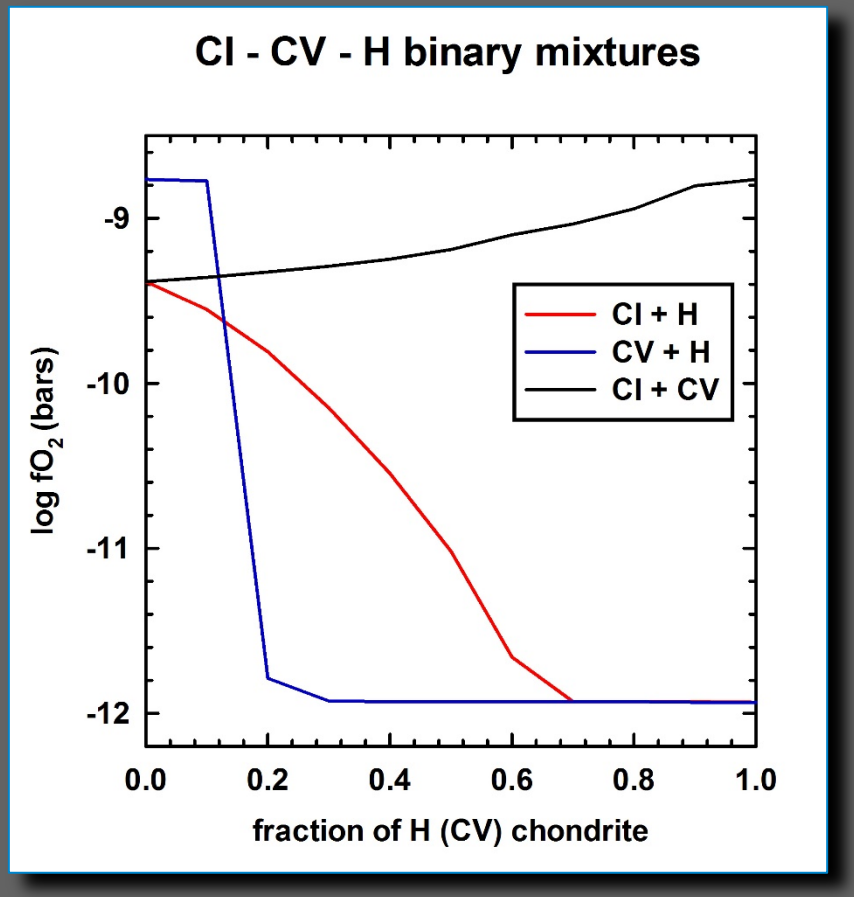

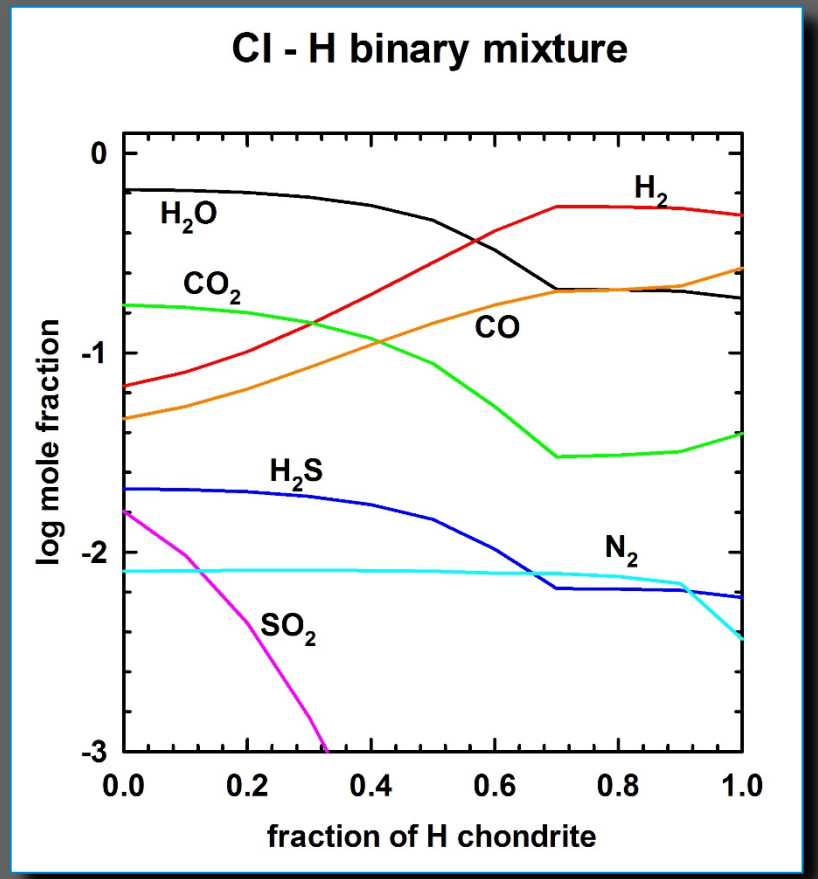

CI – CV – H

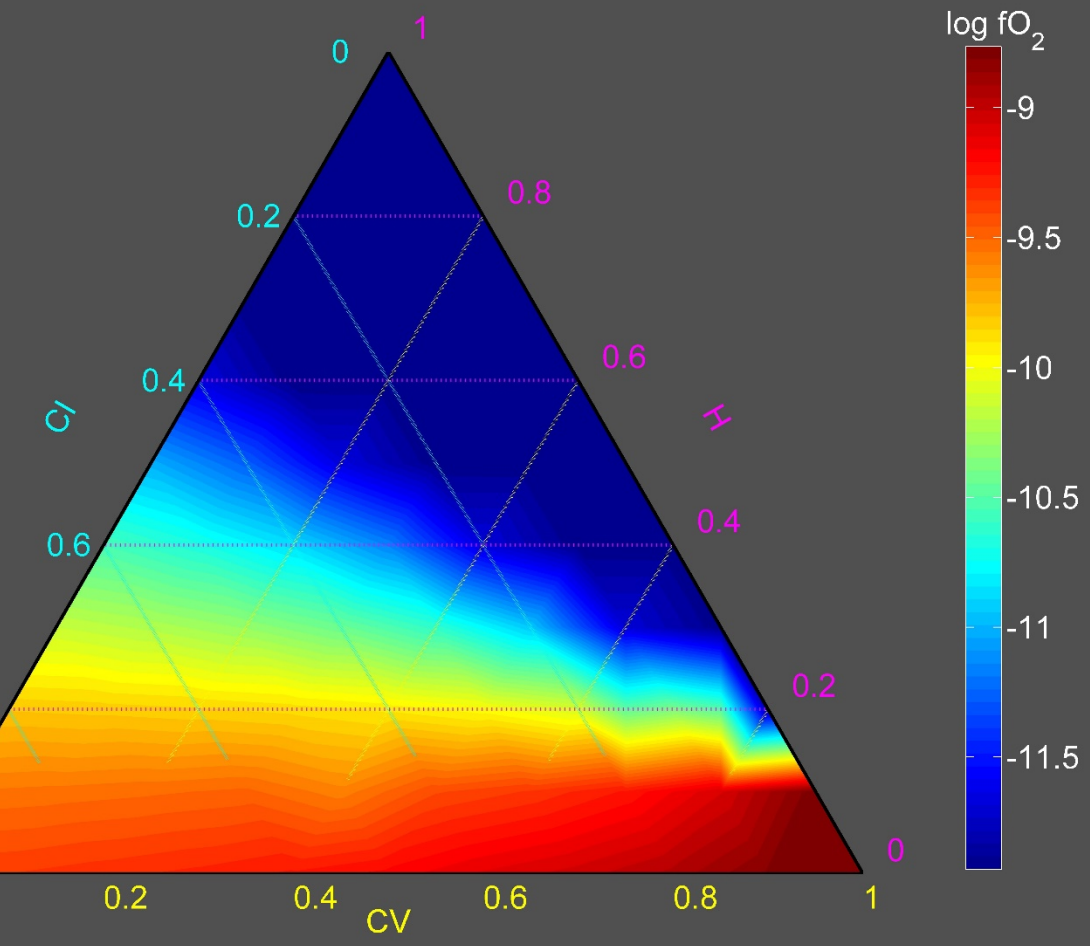

CI – CV – HED

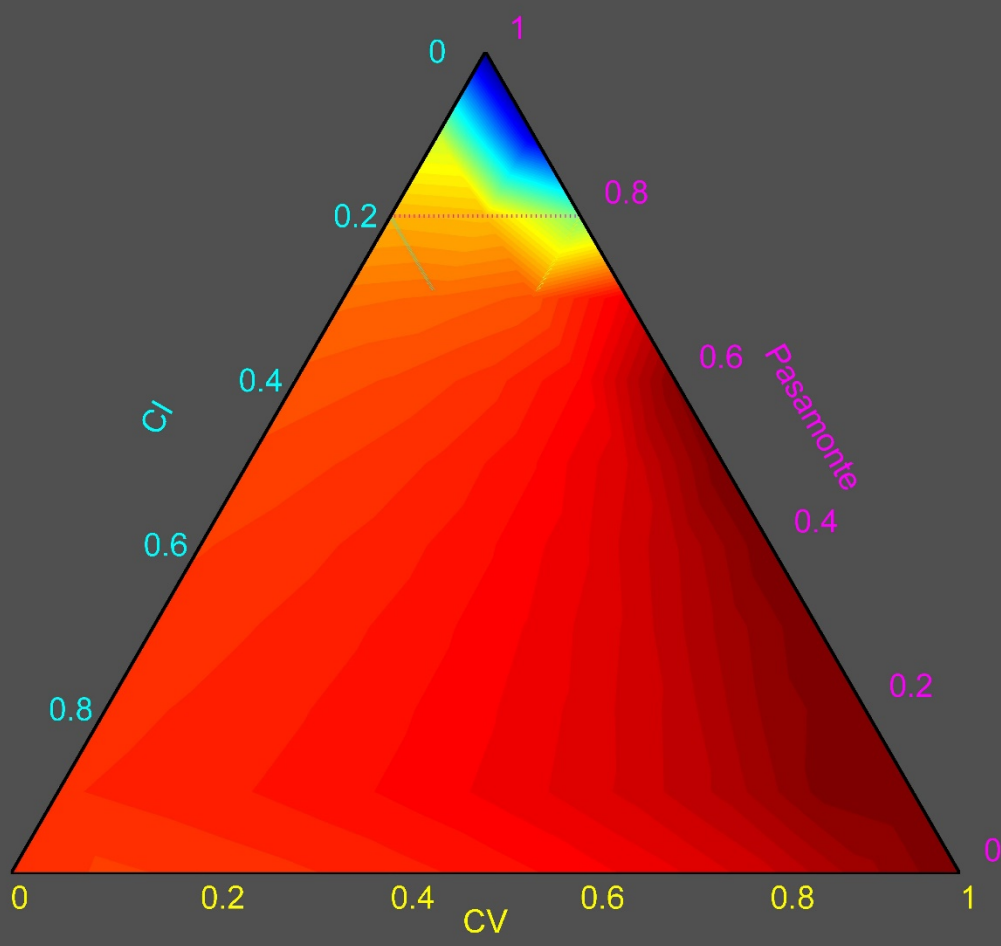

CI – CV – H chondrite ternary mixture